JCTC Journal of Chemical Theory and Computation

General Approach to Compute Vibrationally Resolved One-Photon Electronic Spectra

Julien Bloino,[†,‡] Malgorzata Biczysko,[‡] Fabrizio Santoro,[¶] and Vincenzo Barone*[,†]

Scuola Normale Superiore, piazza dei Cavalieri 7, 56126 Pisa, Italy, Dipartimento di Chimica "Paolo Corradini" and CR-INSTM Village Università di Napoli Federico II, Complesso Universitario Monte S. Angelo, via Cintia, 80126 Napoli, Italy, and Istituto per i Processi Chimico Fisici, Area della Ricerca-CNR, via G. Moruzzi 1, 56124 Pisa, Italy

Received December 16, 2009

Abstract: An effective time-independent approach to compute vibrationally resolved optical spectra from first principles is generalized toward the computation of one-photon electronic spectra induced by either electric or magnetic transition dipoles or by their mutual interaction. These encompass absorption, emission, and circular dichroism spectra. Additionally, the proposed computational scheme is extended to cover a broad range of approximations to evaluate vibronic transitions within both vertical and adiabatic frameworks and to be able to take into account the effects of the temperature. The presented computational tool is integrated into a general purpose computational chemistry package and offers a simple and an easy-to-use way to evaluate one-photon electronic spectra, starting from electronic structure calculations chosen according to the system under study, from fully quantum mechanical descriptions to discrete/continuum quantum mechanical/MM/polarizable continuum models.

1. Introduction

In a recent work,[1] we have presented a versatile procedure to compute vibrationally resolved electronic spectra, when nonadiabatic couplings are negligible, along with its integration into one of the most widely used quantum chemical packages, namely Gaussian.[2] It relies on an efficient a priori prescreening scheme[3,4] to identify the most intense transitions and to generate the spectra of medium-to-large systems[1] at a relatively nonexpensive computational cost. In a first step, the procedure was set within the adiabatic framework and was limited to one-photon absorption (OPA) and emission (OPE) transitions from the vibrational ground state of the initial electronic state, discarding the effects of the temperature. However, our general goal is to provide a robust and easy-to-use computational tool able to assist a broader range of spectroscopic studies. To this purpose, there are several issues which need to be accounted for, like electronic transitions arising from interaction between different transition dipole moments, spectral ranges encompassing more than one final electronic state, temperature effects, and anharmonicity. In the present work, we propose a generalized method able to deal with spectroscopies related either to electric or magnetic transition dipoles or to their mutual interaction. Additionally, we have introduced temperature effects and, in order to extend applicability of the approach to larger systems, also simplified models within the framework of vertical approaches. In such a way, we have completed the formulation and implementation of a general computational tool, set within the harmonic approximation and the time-independent framework, able to simulate zero- and finite-temperature electronic spectra for transitions between two electronic states, showing vibronic effects either negligible or amenable to a description within the Herzberg–Teller intensity-borrowing theory. The following discussion will be limited to OPA, OPE, and electronic circular dichroism (ECD) spectroscopies, in line with the approach[5,6] recently presented by some of us, but our method can also deal with other spectroscopic phenomena, such as the ones

* Corresponding author. E-mail: vincenzo.barone@sns.it.
† Scuola Normale Superiore.
‡ Dipartimento di Chimica "Paolo Corradini" and CR-INSTM Village Università di Napoli Federico II.
¶ Istituto per i Processi Chimico Fisici.

10.1021/ct9006772
Published on Web 03/12/2010

issuing from magnetic dipole moments only. It is noteworthy that similar approaches have also been applied to nonresonant two-photon absorption (TPA) and circular dichroism (TPCD).[7]

Ab initio quantum approaches to the calculation of vibrationally resolved optical spectra require an a priori analysis of the relevant potential energy surfaces (PES), independently of the method adopted to compute the spectrum. However, an extensive analysis of the PES is still impractical, in most cases, and impossible for medium-to-large systems. In the latter, only a local region of the PES about a given geometry can be explored. In generic systems, an electronic excitation can involve any kind of electronic states, including neutral or ionic, and bound or dissociative ones. In addition, the initial and/or final electronic state can be subjected to strong nonadiabatic couplings, as those triggered by the existence of a conical intersection. The probability of occurrence of these couplings increases with the dimension of the system. At the current state-of-the-art, no unique rigorous method can be proposed for such a general situation. It is, therefore, convenient to clarify the reference physical model in which we developed our method: we deal with transitions between nondissociative electronic states not showing conical intersections nor strong noadiabatic effects. In such a framework, if the spectral range of interest encompasses several final electronic states, they are considered uncoupled, and the spectrum can be, therefore, calculated as a sum of the spectra of each of them. As a consequence, it is always possible to focus on a single final state at a time, and we will refer to our approach as a "single-state" approach. In this model, the most natural choice is to build both the initial and final PES, starting from a harmonic analysis at the respective equilibrium geometries. This kind of approach, often referred to as "adiabatic", treats both states on the same foot, i.e. at the same level of accuracy. It is particularly suited for high-resolution descriptions of the spectra, as it simulates correctly most of low- (high-) lying bands of the absorption (emission) spectrum, i.e., transitions to vibrational states spanning the minimum region of the final electronic state PES. Such an approach is especially important when an accurate reproduction of the fine structure of the spectrum is required, in particular, in studies related to the assignment of excited-state frequencies.[8−13] However, an important drawback of this approach is the computational cost of the geometry optimization and the frequency calculations in the excited state, which might be prohibitive for large systems. An alternative model relies on the observation that the most intense transitions are vertical, so that a correct description of the PES of the final state about the geometry of the initial state is more suited to the analysis of the region of the spectral maximum and of the broad features of the low-resolution spectrum. In fact, the latter mostly reflects the short-time dynamics of the system after an instantaneous promotion on the final state. Within the harmonic approximation, such a "vertical" approach describes the final state PES on the ground of its gradient and Hessian at the initial-state equilibrium geometry, so that it has been named VFC (vertical Franck−Condon).[14] Once the initial and final states harmonic PESs are obtained, the machinery to compute the spectra is the same for vertical and adiabatic harmonic models. Therefore, since in most cases, the computation of the excited-state Hessian is the most time-consuming step of the electronic calculation (at least when it is obtained by numerical differentiation of the gradients), the two approaches are about equivalent as far as the computational cost is concerned. From the physical point of view, as discussed above, both have their advantages and drawbacks, but in most cases, when they lead to significantly different results, the harmonic approximation itself is questionable. As an example, the VFC approach shows an increased sensitivity of the Hessian matrix to the anharmonic character of the PES. More generally, when the physical problem under investigation sensibly deviates from the reference single-state harmonic model we introduced above, no rigorous and general solution exists, and each of the adiabatic/vertical frameworks can reveal more suitable than the other for a given specific system. In the case of semirigid molecules showing conical intersections (CI), for instance, the multi-electronic-state problem can be better faced within the so-called linear vibronic coupling model (LVCM), that is based on a diabatic electronic representation and is grounded in the vertical framework. Such a model, that has been developed by the Heidelberg group in a number of seminal contributions,[15,16] is powerful and effective when harmonic approximation is suitable for describing the diabatic PES (notice that CI occurrence always makes adiabatic PES strongly anharmonic), and it has been recently adopted and generalized by Nooijen[17] to one-photon chiral spectroscopies. It is worth highlighting that when conical intersections exist in the region of the coordinate space relevant for the spectral features, attempt to use adiabatic single-state approaches may run into unsurmountable technical problems, as it is clear in the extreme case when the minimum of an adiabatic PES coincides with a CI. Albeit physically relevant, these problems may not appear evident in a vertical single-state approach, simply because the latter does not try to locate the excited-state PES minimum. It is, however, important to clarify that these situations require in principle a multi-electronic-state treatment and, even if a vertical single-state approach is technically affordable, it is not granted that it is also able to catch the main physics of the problem under investigation. From a different perspective, one may recognize that the exploration of the excited-state PES necessary to locate the excited minima can bring to light issues and problems that may simply remain unobserved in a vertical approach.

At the current state-of-the-art, the most effective implementation of LVCM for spectra calculation is based on time-dependent methods, like the multiconfigurational time-dependent Hartree (MCTDH),[18] even if time-independent (e.g., Lanczos-based) treatments are possible for limited-dimensionality problems (up to a dozen of modes) and if promising Green-function approaches have been recently proposed.[19] In the present paper, we do not deal with nonadiabatic problems, and our work is focused on the development of a robust tool for single-state harmonic spectra that can be used also by non specialists. Within this chosen framework, beyond adiabatic methods, we found it conve-

nient to implement a simplified vertical model, by assuming that the Hessian matrix is the same in both initial and final states. Such a model, which we will refer to as vertical gradient (VG), is also known in literature as the linear coupling model (LCM)[20] (which, nonetheless, should not be confused with the multistate LVCM approach introduced above.)[15,16] In VG, only the energy gradients need to be evaluated in the final state at the equilibrium geometry of the initial one, a task much less time-consuming than the Hessian computation.

Up to now, we have discussed possible deviations from our reference physical model, arising from nonadiabatic couplings. Another issue of general relevance to be dealt with is anharmonicity. It is worthy to highlight, in fact, that its proper consideration is by far more complicated here than in vibrational spectroscopy since one has to deal contemporarily with two different electronic states. As a matter of fact, equilibrium geometries could be quite different, and this requires the description of a larger amount of the PES with the consequent problems of couplings, limits of polynomial expansions, etc. Furthermore, the normal modes of the two states can be sufficiently different to require the inclusion of large sets of coupling terms, which cause additional methodological and numerical difficulties. Moreover, minimization of coupling terms is often nonoptimal when normal modes are expressed in Cartesian coordinates, and switching to internal coordinates could be more effective.[21,22] While this is quite straightforward for small systems and/or well-defined modes, a general and automatized procedure for large systems is still lacking. This is the reason why we prefer deferring the issue of anharmonicity to further work, after we have developed a general and robust strategy at the harmonic level. Nonetheless, when anharmonicity can be considered nearly "diagonal" in terms of the normal modes of the reference state, at least two effective procedures have been proposed for semirigid systems[8] and for cases involving a single anharmonic mode,[14] respectively. The current approach incorporates a simple scheme to correct vibronic transitions for the anharmonicity in the case of semirigid systems.

In the above discussion, we have explicitly settled our reference physical model. Despite the discussed limitations, this model is able to provide a reliable interpretation of the electronic spectroscopy data for a very broad range of molecular species. On the other hand, the elaboration of a general and robust method, along with its implementation, still needs to be considered a very challenging part of the computational spectroscopy field. To this purpose, two main and strictly correlated issues must be taken into proper account, the former concerns the reliability of the electronic description, while the latter is more focused on the vibrational problem. More specifically, the first issue related to the evaluation of properties of molecular systems in their excited electronic states affects the reliability of computational spectroscopy studies. In fact, until recently, computations of vibronic spectra have been limited to small molecules, but recent developments in electronic structure theory for excited states within the time-dependent density functional theory (TD-DFT)[23,24] and the resolution of the identity approximation of coupled cluster theory (RI-CC2)[25] have paved the route toward the simulation of spectra for significantly larger systems. In this respect, a pivotal role can be played by hybrid DFT/CC approaches where the most expensive computationally geometry optimization and Hessian computations are performed by DFT with medium-size basis sets, while energies and/or other properties can be computed with more accurate quantum mechanics (QM) approaches.[8] However, when larger systems are to be studied, besides the QM treatment, a second computational challenge arises from the inclusion of vibrational contributions. Indeed, the number of vibrational states to be taken into account increases steeply with the dimension of the system and with the spectral width, but most of the possible vibronic transitions do not contribute significantly to the spectrum and can be safely neglected. Therefore, wise and effective selection criteria to individuate a priori the most relevant vibronic transitions within the dense bath of possible final states can make feasible the calculations of spectrum lineshapes for macromolecular systems. Several schemes have been proposed[3,26−30] ranging from the simplest approach, based solely on the energy window of the spectrum,[26,27] up to rigorous prescreening techniques, based on analytically derived sum rules.[30] In order to maximize the efficiency of calculations and to deal with large systems, it is necessary to adopt a fast, a priori selection scheme of general applicability for a variety of different systems that is able to correctly choose all the non-negligible transitions. We have recently derived a general and robust tool rooted into a method recently introduced by some of us[3,29] in the frame of harmonic approximation, which has been proven to provide very accurate spectra of medium-to-large systems with a limited computational cost.[8] Moreover, in the implementation,[1] particular care has been taken to avoid the introduction of any built-in restriction, be it for the number of allowed quanta in a single mode, for the number of simultaneously excited vibrations, or for the spectrum energy range. In this paper, we extend the applicability of our tool to other spectroscopic phenomena, temperature effects, and even larger systems (through the VG model). Thanks to the new available features and to the full integration into the Gaussian package, the one-photon electronic spectra for a wide variety of cases can be treated in a fully automatic way easily accessible also to nonspecialists. In this work, the developed tool is applied to a variety of different systems and problems, such as simulations of OPA, OPE, and ECD spectra with and without temperature effects and both in the gas phase and in solution (where the solvent is described within polarizable continuum models).

The paper is organized as follows: Section 2 describes the theoretical frame of the generalized approach to compute one-photon electronic spectra, along with the details of the current implementation. Computational models, which have been applied to the determination of structures, forces, vibrations, and energies to provide the information necessary for spectra calculation, are gathered in Section 3. The developed method gave us the opportunity to extensively validate the DFT/N07 model for the computations of ECD spectra, and results are reported in Section 4. Finally, the simulated vibrationally resolved one-photon electronic spectra are gathered in Section 5. Aspects of simulated spectra convergence are discussed in Sections 5.1 and 5.2 on the

example of the well studied $S_2 \leftarrow S_0$ one-photon ECD spectrum of (*R*)-(+)-3 methylcyclopentanone (R3MCP), which is followed by two illustrative examples of direct application of our integrated approach to larger systems: the UV−vis absorption spectrum in the 250−700 nm range of chlorophyll a1 (Section 5.3) in methanol solution, and the ECD spectrum of $\pi^* \leftarrow n$ transition of (*Z*)-8-methoxy-4-cyclooctenone (MCO) (Section 5.4).

2. Computation of One-Photon Electronic Spectra

2.1. Generalized Model. In order to deal with different one-photon electronic spectroscopies, the procedure described in our previous work[1] has been redesigned to be as general as possible. Additionally, it has been modified to provide quantities easier to compare with their experimental counterparts. In this context, the intensity of OPA, fluorescence, OPE and ECD can be expressed by the same equation:

$$I = \alpha\omega^{\beta} \sum_m \sum_n \rho_\gamma [\boldsymbol{d}_{\mathrm{A}mn} \cdot \boldsymbol{d}^*_{\mathrm{B}mn}] \delta(\omega_n - \omega_m - \omega) \quad (1)$$

where the symbol "*" is used to represent the conjugate of $\boldsymbol{d}_{\mathrm{B}mn}$, and δ is the Dirac function.

The quantity I is evaluated by taking into account all transition probabilities, represented by the double summation over all possible initial vibronic states m, weighted by the probability of the molecule to be in this initial state given by the Boltzmann population ρ_γ and by the final vibronic states n.

The intensity for OPA, OPE, or ECD is given by replacing I, α, β, γ, $\boldsymbol{d}_{\mathrm{A}mn}$, and $\boldsymbol{d}_{\mathrm{B}mn}$ with the values given in the list below:

$$\text{OPA: } I = \varepsilon(\omega),\ \alpha = \frac{10\pi\mathcal{N}_{\mathrm{A}}}{3\varepsilon_0 \ln(10)\hbar c},\ \beta = 1,\ \gamma = m,\ \boldsymbol{d}_{\mathrm{A}mn} = \boldsymbol{d}_{\mathrm{B}mn} = \boldsymbol{\mu}_{mn}$$

$$\text{OPE: } I = I_{em}/N_n,\ \alpha = \frac{2\mathcal{N}_{\mathrm{A}}}{3\varepsilon_0 c^3},\ \beta = 4,\ \gamma = n,\ \boldsymbol{d}_{\mathrm{A}mn} = \boldsymbol{d}_{\mathrm{B}mn} = \boldsymbol{\mu}_{mn}$$

$$\text{ECD: } I = \Delta\varepsilon(\omega),\ \alpha = \frac{40\mathcal{N}_{\mathrm{A}}\pi}{3\varepsilon_0 \ln(10)\hbar c^2},\ \beta = 1,\ \gamma = m,\ \boldsymbol{d}_{\mathrm{A}mn} = \boldsymbol{\mu}_{mn},\ \boldsymbol{d}_{\mathrm{B}mn} = \mathcal{I}(\boldsymbol{m}_{mn})$$

where $\varepsilon(\omega)$ is the molar absorption coefficient for a given angular frequency ω, $\Delta\varepsilon(\omega)$ is the difference (referred to as anisotropy) between the molar absorption coefficients ε^- and ε^+, relative to the left and right circularly polarized light, respectively. For OPE, I_{em}/N_n is the energy emitted by one mole per second. It is noteworthy that phosphorescence spectra, i.e., emission from electronic states characterized by different spin multiplicity with respect to the ground electronic state, depend on spin−orbit couplings that are not always available. In this case, only Franck−Condon calculations are performed (see below for details), assuming the transition is fully allowed with the length of the electric transition dipole moment set to 1 au.

Finally, $\mathcal{N}_{\mathrm{A}}$ is the Avogadro constant, ε_0 is the vacuum permittivity, $\boldsymbol{\mu}_{mn}$ is the electric transition dipole moment between the vibronic states m and n, and $\mathcal{I}(\boldsymbol{m}_{mn})$ is the imaginary part of the magnetic transition dipole moment between the vibronic states m and n, $\boldsymbol{m}_{mn}$. A more detailed description of the calculation of I for OPA, OPE, and ECD is available in ref 31.

We will use from now on the symbol $\boldsymbol{d}_{\mathrm{X}}$ to represent indifferently $\boldsymbol{d}_{\mathrm{A}}$ and $\boldsymbol{d}_{\mathrm{B}}$. We define the integral $\boldsymbol{d}_{\mathrm{X}mn}$ and its conjugate as

$$\boldsymbol{d}_{\mathrm{X}mn} = \langle \Psi_m | \boldsymbol{d}_{\mathrm{X}} | \Psi_n \rangle \quad (2)$$

$$\boldsymbol{d}^*_{\mathrm{X}mn} = \langle \Psi_n | \boldsymbol{d}^*_{\mathrm{X}} | \Psi_m \rangle \quad (3)$$

where Ψ_m and Ψ_n are the molecular wave functions of the vibronic states m and n, respectively.

From eq 1, one can see that the knowledge of I is bound to the evaluation of $\boldsymbol{d}_{\mathrm{A}mn} \cdot \boldsymbol{d}_{\mathrm{B}mn}{}^*$.

In the framework of the Born−Oppenheimer approximation, the molecular wave function Ψ can be written as a product of its electronic and nuclear components, ψ_{e} and ψ_{N}, respectively. For readability, the spectroscopic convention will be used to designate the wave functions, a single quote ($'$) representing the lower vibronic state in energy m and a double quote ($''$) the higher state, n.

$$\langle \Psi' | \boldsymbol{d}_{\mathrm{X}} | \Psi'' \rangle = \langle \psi'_{\mathrm{e}} \psi'_{\mathrm{N}} | \boldsymbol{d}^{\mathrm{e}}_{\mathrm{X}} | \psi''_{\mathrm{e}} \psi''_{\mathrm{N}} \rangle + \langle \psi'_{\mathrm{e}} \psi'_{\mathrm{N}} | \boldsymbol{d}^{\mathrm{N}}_{\mathrm{X}} | \psi''_{\mathrm{e}} \psi''_{\mathrm{N}} \rangle \quad (4)$$

Because of the orthogonality of the electronic wave functions, the second term in the right-hand side (rhs) of the previous equation is null, so that:

$$\langle \Psi' | \boldsymbol{d}_{\mathrm{X}} | \Psi'' \rangle = \langle \psi'_{\mathrm{e}} \psi'_{\mathrm{N}} | \boldsymbol{d}^{\mathrm{e}}_{\mathrm{X}} | \psi''_{\mathrm{e}} \psi''_{\mathrm{N}} \rangle = \langle \psi'_{\mathrm{N}} | \boldsymbol{d}^{\mathrm{e}}_{\mathrm{X}mn} | \psi''_{\mathrm{N}} \rangle \quad (5)$$

Finally, assuming that the Eckart conditions[32] are met, it is possible to separate, with a good approximation, the nuclear wave function into translational, rotational, and vibrational terms. As we are interested in the vibrational contribution in radiative transitions, we discard the translational and rotational wave functions:

$$\langle \Psi' | \boldsymbol{d}_{\mathrm{X}} | \Psi'' \rangle = \langle \psi'_v | \boldsymbol{d}^{\mathrm{e}}_{\mathrm{X}mn} | \psi''_v \rangle$$

More precisely, the intensity in eq 1 is obtained after an orientational averaging that assumes freely rotating molecules. The electric and magnetic transition dipole moments, $\boldsymbol{\mu}^e_{mn}$ and $\boldsymbol{m}^e_{mn}$ respectively, are, in general, unknown functions of the vibrational coordinates so that the transition dipole moment $\boldsymbol{d}^{\mathrm{e}}_{\mathrm{X}mn}$, which could represent either $\boldsymbol{\mu}^{\mathrm{e}}_{mn}$ or $\mathcal{I}(\boldsymbol{m}^{\mathrm{e}}_{mn})$, must be approximated. The most common approximation, stated by Franck[33] and formalized by Condon,[34] assumes that the transition takes place in such a short time that the position of the nuclei remains almost unchanged and that the transition dipole can be considered as constant. While this approximation is fairly good when the transition is fully allowed and the minima of the potential energy surfaces of the initial and final electronic states are almost vertically to each other, it shows serious limitations when the transition is weakly allowed or dipole forbidden. The limitation is even

more strongly felt for ECD where the product $\boldsymbol{\mu}_{mn}\cdot\mathscr{T}(\boldsymbol{m}_{mn})$ can be almost negligible, even if the transition is strongly allowed whenever the electric and magnetic moments are nearly orthogonal. An early extension to the Franck−Condon principle was proposed by Herzberg and Teller[35] and accounted for a linear variation of the transition dipole moment, with respect to the normal coordinates of the initial state, $\boldsymbol{Q}'$ or $\boldsymbol{Q}''$, depending if absorption or emission is considered. It must be recognized, however, that, once the most suitable physical model has been chosen and the proper quantities obtained from electronic calculations (e.g., from the expansion around the initial-state geometry), from the mathematical point of view, the transition dipole moment $\boldsymbol{d}^{e}_{Xmn}$ can be equally well expressed in a Taylor expansion around the equilibrium geometry of each electronic state. For convenience, with respect to the formulation of the overlap integrals in the rest of the document, the higher state in energy is chosen as the reference. The Taylor expansion about the equilibrium geometry of this state, $\boldsymbol{Q}''_0 = \boldsymbol{0}$, is

$$\boldsymbol{d}^{e}_{Xmn}(\boldsymbol{Q}'') \approx \boldsymbol{d}^{e}_{Xmn}(\boldsymbol{Q}''_0) + \sum_{i=1}^{N}\left(\frac{\partial \boldsymbol{d}^{e}_{Xmn}}{\partial Q''_i}\right)_0 Q''_i + \frac{1}{2}\sum_{i=1}^{N}\sum_{j=1}^{N}\left(\frac{\partial^2 \boldsymbol{d}^{e}_{Xmn}}{\partial Q''_i \partial Q''_j}\right)_0 Q''_i Q''_j + \ldots \quad (6)$$

where N is the number of normal modes.

The FC approximation corresponds to the first term in the rhs of eq 6, HT to the second one and Franck−Condon Herzberg−Teller (FCHT) to both terms. The remaining terms in eq 6 will not be taken into account in the following discussion. From a vibronic point of view, the HT term introduces an intensity borrowing effect due to the interaction of the states involved in the electronic transition with other closely lying electronic states, with which they mix upon small displacements along the normal coordinates. When an electronic multistate diabatic representation is adopted, like in the linear coupling vibronic model cited in Section 1 (the Introduction), Herzberg−Teller effects are usually less important since diabatic states are defined in order to be ideally independent of the coordinates. In those cases, intensity borrowing mechanisms are explicitly introduced by the coupling among the different diabatic states. However, when the interacting states are sufficiently separated in energy and when the interaction is weak, traditional HT treatment allows to account for the main borrowing effects, keeping the simplicity of an adiabatic single-state description.

At this stage, it is useful to digress from the theoretical background and to take a deeper look into the computational implementation. While our method is fully general and can be applied starting from data obtained with any electronic model, it is oriented toward large molecules. It must be recognized that the state of the art methods rooted to TD-DFT provide probably the most effective route to treat such systems. In this approach, the excited-state Hessian, required for harmonic analysis, is computed by numerical differentiation of the energy gradient at the equilibrium geometry of the excited state. During this calculation, it is also possible to obtain, at no additional cost, the numerical derivatives of the electric and magnetic transition dipole moments. Therefore, by default, our implementation uses these sets of data for HT and FCHT calculations. It must be remembered, however, that, as previously discussed in ref 4, Herzberg and Teller considered in their original work[35] the initial state as the state of reference for the linear variation of the electronic transition dipole moment (we call it ^{i}HT), in line with the FC principle. Therefore, while fully agreeing with their original approach for emission, our default computational implementation slightly differs from their original proposal for absorption processes, adopting the final-state equilibrium geometry reference (^{f}HT). It should be noted that nondefault choices of proper keywords allow a calculation along the original ^{i}HT formulation, to be performed also for absorption processes. However, we point out that when the ^{i}HT and ^{f}HT approaches lead to substantial different results, the common linear approximation must probably be questioned.

Regarding the vertical gradient (VG) approach, it is possible to combine it with the FC and the FCHT approximations, as often done in the literature.[20] Nonetheless, at least at the TD-DFT level, the effort required for the numerical differentiation of the transition dipole derivatives neutralizes the computational convenience of the VG model, since at the same cost the excited state normal modes also can be obtained. Hence, in the following, the VG is only adopted in combination with the FC approximation.

Using eq 6, the transition dipole moment integral $\boldsymbol{d}_{Xmn}$ is given by the relation

$$\langle \Psi_m | \boldsymbol{d}_x | \Psi_n \rangle \approx \boldsymbol{d}^{e}_{Xmn}(\boldsymbol{Q}''_0)\langle \psi'_v | \psi''_v \rangle + \sum_{i=1}^{N}\left(\frac{\partial \boldsymbol{d}^{e}_{Xmn}}{\partial Q''_i}\right)_0 \langle \psi'_v | Q''_i | \psi''_v \rangle \quad (7)$$

The overlap integral $\langle \psi'_v | \psi''_v \rangle$ is also referred as the Franck−Condon integral.

While the treatment can be done at the anharmonic level,[36,37] our current implementation treats the calculation of the Franck−Condon integrals at the harmonic level. With this approximation, the multidimensional wave function ψ_v can be written as a product of one-dimensional vibrational wave functions ψ_{v_i},

$$|\psi_v\rangle = \prod_{i=1}^{N} |\psi_{v_i}\rangle \quad (8)$$

For purposes of compactness, the convenient Dirac notation will be adopted from now on, $|\psi_v\rangle = |\boldsymbol{v}\rangle$ where v represents the vector of quantum numbers v_i for each vibrational mode i.

Using second quantization, the second term in the rhs of eq 7, which depends on the normal coordinates $\boldsymbol{Q}''$, can be reformulated as

$$\langle \boldsymbol{v}' | Q''_i | \boldsymbol{v}'' \rangle = \sqrt{\frac{\hbar}{2\omega''_i}}\left[\sqrt{v''_i}\langle \boldsymbol{v}' | \boldsymbol{v}'' - 1''_i \rangle + \sqrt{v''_i + 1}\langle \boldsymbol{v}' | \boldsymbol{v}'' + 1''_i \rangle\right] \quad (9)$$

Table 1. Ab Initio Computations Required to Generate the Input Data for the Simulation Vibrationally Resolved Electronic Spectra with the VG, AS, AFC, and AFCHT Models

computation	VG[a]	AS[a]	AFC	AFCHT
initial state				
Cartesian coordinates of the atoms (equilibrium structure)	x	x	x	x
energy at the minimum of the PES (equilibrium geometry)	x	x	x	x
frequencies	x	x	x	x
normal modes, expressed by the atomic displacements	x	x	x	x
final state				
Cartesian coordinates of the atoms at the minimum of the PES (equilibrium structure)		x	x	x
energy at the equilibrium geometry of the initial state	x			
energy at the minimum of the PES (equilibrium geometry)		x	x	x
forces at the equilibrium geometry of the initial state	x			
frequencies			x	x
normal modes, expressed by the atomic displacements			x	x
general				
atomic masses	x	x	x	x
transition dipole moments	x	x	x	x
derivatives of the transition dipole moments				x

[a] For the VG and AS approaches, it is assumed that the FC approximation is used. See text for the details.

Introducing eq 9 in eq 7, we obtain the following Taylor expansion for the transition dipole moment:

$$\langle \Psi_m | \boldsymbol{d}_x | \Psi_n \rangle \approx \boldsymbol{d}^{e}_{Xmn}(\boldsymbol{Q}''_0)\langle v' | v'' \rangle + \sum_{i=1}^{N} \left(\frac{\partial \boldsymbol{d}^{e}_{Xmn}}{\partial Q''_i} \right)_0 \sqrt{\frac{\hbar}{2\omega''_i}} [\sqrt{v''_i}\langle v' | v'' - 1''_i \rangle + \sqrt{v''_i + 1}\langle v' | v'' + 1''_i \rangle] \tag{10}$$

A major issue to calculate the integrals in eq 10 arises from the fact that each vibrational wave function is expressed in a different set of normal coordinates. This problem can be overcome by the linear transformation proposed by Duschinsky[38] to express the normal coordinates of one state with respect to the other's:

$$\boldsymbol{Q}^i = \boldsymbol{J}\boldsymbol{Q}^f + \boldsymbol{K} \tag{11}$$

where $\boldsymbol{J}$ is the so-called Duschinsky matrix and represents the mixing of the normal modes during the transition, and $\boldsymbol{K}$ is the shift vector of the normal modes between the initial and final states. $\boldsymbol{Q}^i$ represents the normal coordinates of the initial state, and $\boldsymbol{Q}^f$ represents those of the final one. In case of OPA or ECD spectroscopies, $\boldsymbol{Q}^i = \boldsymbol{Q}'$ and $\boldsymbol{Q}^f = \boldsymbol{Q}''$, and in OPE, $\boldsymbol{Q}^i = \boldsymbol{Q}''$ and $\boldsymbol{Q}^f = \boldsymbol{Q}'$.

The rotation or Duschinsky matrix is given by

$$\boldsymbol{J} = (\boldsymbol{L}^i)^{-1}\boldsymbol{L}^f \tag{12}$$

where $\boldsymbol{L}^i$ and $\boldsymbol{L}^f$ are the transformation matrices from mass-weighted Cartesian coordinates to normal coordinates of the initial and final states, respectively.

When considering an adiabatic model, the shift vector is given by the difference of geometries between the final and initial states:

$$\boldsymbol{K} = (\boldsymbol{L}^i)^{-1}\boldsymbol{M}^{1/2}\Delta\boldsymbol{X} \tag{13}$$

where $\boldsymbol{M}$ is the diagonal matrix of atomic masses, and $\Delta\boldsymbol{X} = \boldsymbol{X}_0{}^f - \boldsymbol{X}_0{}^i$ is a vector representing the shift of nuclear Cartesian coordinates between the initial ($\boldsymbol{X}^i$) and final ($\boldsymbol{X}^f$) states.

For "vertical" models, the structure remains unchanged, but information about the shift of the normal modes between the initial and final states are obtained from the energy gradient in the final state. Since our treatment of the vertical models will be limited here to VG, we report only the shift used for this approximation:

$$\boldsymbol{K} = -\{\boldsymbol{\Omega}^i\}^{-2}[(\boldsymbol{L}^i)^{-1}\boldsymbol{M}^{-1/2}\boldsymbol{g}^f] \tag{14}$$

where $\boldsymbol{\Omega}^i$ is the diagonal matrix of the harmonic frequencies $\boldsymbol{\omega}$ of the initial state, and $\boldsymbol{g}^f$ is the final state's energy gradient in Cartesian coordinates.

It should be noted that in this model, the Hessian matrix of the final state is assumed to be the same as in the initial state. As a consequence, we have $\boldsymbol{L}^i = \boldsymbol{L}^f$ so that $\boldsymbol{J}$ is the identity matrix $\boldsymbol{I}$. Moreover, it is assumed that the final-state frequencies are identical to the initial-state ones. Based on these approximations, we can also define an "adiabatic" model, that we will refer to as adiabatic shift, where $\boldsymbol{J}$ is replaced by the identity matrix while the shift vector $\boldsymbol{K}$ is kept unchanged with respect to the value given in eq 13. Notice that, at variance with the adiabatic models where the shift vector only depends on structural parameters (the two equilibrium geometries), thus representing a true displacement, in VG $\boldsymbol{K}$ not only depends on the vibrational frequencies of the initial state but it is also sensitive to anharmonicities (through the gradient), and it must be considered, therefore, a sort of "effective displacement".

The overlap integrals can then be evaluated analytically[39−44] or recursively.[45−48] While the former method allows straightforward calculations and avoids possible error propagation, it suffers from a quickly growing complexity and a lack of versatility when dealing with medium-to-large systems. As a consequence, the more general-purpose recursive approach presented by Ruhoff[47] and based on the generating functions of Sharp and Rosenstock[39] has been implemented:

$$\langle v'|v''\rangle = \frac{1}{\sqrt{2v_i'}}\left[B_i\langle v' - 1_i'|v''\rangle + \sqrt{2(v_i' - 1)}A_{ii}\langle v' - 2_i'|v''\rangle + \sum_{j=1,j\neq i}^{N}\sqrt{2v_j'}A_{ij}\langle v' - 1_i' - 1_j'|v''\rangle + \sum_{j=1}^{N}\sqrt{\frac{v_j''}{2}}E_{ji}\langle v' - 1_i'|v'' - 1_j''\rangle\right] \quad (15)$$

and

$$\langle v'|v''\rangle = \frac{1}{\sqrt{2v_i''}}\left[D_i\langle v'|v'' - 1_i''\rangle + \sqrt{2(v_i'' - 1)}C_{ii}\langle v'|v'' - 2_i''\rangle + \sum_{j=1,j\neq i}^{N}\sqrt{2v_j''}C_{ij}\langle v'|v'' - 1_i'' - 1_j''\rangle + \sum_{j=1}^{N}\sqrt{\frac{v_j'}{2}}E_{ij}\langle v' - 1_j'|v'' - 1_i''\rangle\right] \quad (16)$$

where the matrices and vectors **A**, **B**, **C**, **D**, and **E** are the Sharp and Rosenstock matrices.

2.2. An Efficient A Priori Method to Generate One-Photon Electronic Spectra. Once the final electronic state is individuated, no selection rule (beyond those based on the symmetry of the vibrational wave functions) exists to effectively limit the huge number of possibly bound final states to be taken into account in sizable molecules. However, transitions to most of them have a negligible intensity. Based on this observation, a prescreening method[3,4] is used to select a priori the most intense transitions. It relies on a categorization of the latter with respect to the number of simultaneously excited modes in the final state, called classes. For instance, class 1 ($\mathcal{C}_1$) represents all transitions to final vibrational states with a single excited mode i, $\langle v'|\mathbf{0}'' + v_i''\rangle$, and class 0 contains the overlap integral between the vibrational ground states, $\langle \mathbf{0}'|\mathbf{0}''\rangle$. Based on this division, the overlap integrals in classes 1 and 2 are used as reference data to prescreen those to compute in each "higher" class, each class being calculated one after the other, increasing the number of excited modes in the final state. The advantages of using the overlap integrals of these classes are two-fold. The first one is that these integrals are computationally cheap and are generated quickly even in the case of large molecules. The second interest lies in the information provided by the reference data. We present here a generalized approach able to handle OPA, OPE, and ECD spectroscopies, but which could be extended easily to additional kinds of spectroscopy.

Depending if only the zeroth order of the Taylor expansion given in eq 6 or higher orders are considered, two or three data sets are required. This number is doubled when temperature is taken into account. The first general set, $F_{\mathcal{C}_1}$, is defined during the calculation of the transtions from class 1. Its elements are defined as

$$F_{\mathcal{C}_1}(i, v_i'') = \left|\frac{1}{\sqrt{2v_i''}}\left[D_i\langle \mathbf{0}'|\mathbf{0}'' + v_i'' - 1_i''\rangle + \sqrt{2(v_i'' - 1)}C_{ii}\langle \mathbf{0}'|\mathbf{0}'' + v_i'' - 2_i''\rangle\right]\right|^2 \quad (17)$$

where the factors C_{ii} and D_i give, respectively, information on the effect of the shifts in equilibrium positions and the frequency changes on the overlap integrals of overtones and, more precisely, on the vibrational progression of mode i.

The second set, $F_{\mathcal{C}_2}$, is obtained in class 2 and gives information about the Duschinsky mixing of the normal modes. It contains all combinations of modes i and j but only considering the cases of an equal number of quanta for both modes ($v_i'' = v_j''$):

$$F_{\mathcal{C}_2}(i, j, v_i'' = v_j'') = |\langle \mathbf{0}'|\mathbf{0}'' + v_i'' + v_j''\rangle|^2 - \frac{F_{\mathcal{C}_1}(i, v_i'') \times F_{\mathcal{C}_1}(j, v_i'')}{|\langle \mathbf{0}'|\mathbf{0}''\rangle|^2} \quad (18)$$

For Herzberg−Teller calculations (HT or FCHT approximations), a second data set is extracted from class 1, $H_{\mathcal{C}_1}$, which stores an upper-bound estimation of the square of the pure Herzberg−Teller contribution for a given mode i and the corresponding transition $\langle \mathbf{0}'|\mathbf{0}'' + v_i''\rangle$:

$$\begin{aligned} H_{\mathcal{C}_1}(i, v_i'') &= \sum_{\tau=x,y,z}\left|\left(\frac{\partial \boldsymbol{d}^{e}_{Amn}(\tau)}{\partial Q_i''}\right)_0\right|\left|\left(\frac{\partial \boldsymbol{d}^{e*}_{Bmn}(\tau)}{\partial Q_i''}\right)_0\right| \\ &\times \left|\sqrt{\frac{\hbar}{2\omega_i''}}[\sqrt{v_i''}\langle \mathbf{0}'|\mathbf{0}'' + v_i'' - 1_i''\rangle + \sqrt{v_i'' + 1}\langle \mathbf{0}'|\mathbf{0} + v_i'' + 1_i''\rangle]\right|^2 \end{aligned} \quad (19)$$

with the summation over each Cartesian coordinate of the transition dipole moments $\boldsymbol{d}^{e}_{Amn}$ and $\boldsymbol{d}^{e}_{Bmn}$.

The method to choose the maximum quantum number of each mode has been extensively presented in previous references.[3,4]

When considering temperature, an additional difficulty lies in the choice of the starting vibrational states in the initial electronic state. An evident way to limit the treatment is to use a threshold on the Boltzmann population of each vibrational state. In practice, this threshold is set with respect to the population of the ground state. Similarly to the final states, a division in classes is performed for the initial states. For each class, a set is defined by the initial states sharing the same simultaneously excited modes, so that they differ only by the quantum numbers of these modes, and each set (in previous papers named "mother states")[4,29] is treated separately. The a priori selection of the most intense transitions requires two additional (or

three in the case of the Herzberg−Teller approximation) data sets, $F^{T}_{\mathcal{G}_1}$ and $F^{T}_{\mathcal{G}_2}$ (and $H^{T}_{\mathcal{G}_1}$), which are equivalent to $F_{\mathcal{G}_1}$ and $F_{\mathcal{G}_2}$ (and $H_{\mathcal{G}_1}$) for the case of finite temperature. These sets are defined for the highest-energy initial state for each set:

$$F^{T}_{\mathcal{G}_1}(i, v_i'') = \left|\frac{1}{\sqrt{2v_i''}}\left[D_i\langle v'|0'' + v_i'' - 1_i''\rangle + \sqrt{2(v_i'' - 1)}C_{ii}\langle v'|0'' + v_i'' - 2_i''\rangle + \sum_{j=1}^{N}\sqrt{\frac{v_j'}{2}}E_{ij}\langle v' - 1_j'|0'' + v_i'' - 1_i''\rangle\right]\right|^2 \quad (20)$$

$$F^{T}_{\mathcal{G}_2}(i, j, v_i'' = v_j'') = |\langle v'|0'' + v_i'' + v_i''\rangle|^2 - \frac{F^{T}_{\mathcal{G}_1}(i, v_i'') \times F^{T}_{\mathcal{G}_1}(j, v_i'')}{|\langle v'|0''\rangle|^2} \quad (21)$$

$$H^{T}_{\mathcal{G}_1}(i, v_i'') = \sum_{\tau=x,y,z}\left|\left(\frac{\partial d^{e}_{Amn}(\tau)}{\partial Q_i''}\right)_0\right|\left|\left(\frac{\partial d^{e}_{Bmn}{}^{*}(\tau)}{\partial Q_i''}\right)_0\right| \times \left|\sqrt{\frac{\hbar}{2\omega_i''}}\left[\sqrt{v_i''}\langle v'|0'' + v_i'' - 1_i''\rangle + \sqrt{v_i'' + 1}\langle v'|0 + v_i'' + 1_i''\rangle\right]\right|^2 \quad (22)$$

Details of the prescreening method when taking into account the temperature can be found in ref 29.

When choosing a priori the transitions to compute, it is necessary to control the reliability of this prescreening. This is done by comparing the total intensity I^{calc} obtained by the addition of all the transitions taken into account to the expected intensity I^{tot} calculated using analytic sum rules.

The method to compute the "analytic" total intensities has been presented in previous papers, approximating the electronic transition dipole moment in a Taylor series up to the second order.[1,4] For completeness, we report the generalized calculation of the spectrum convergence (I^{calc}/I^{tot}) for any couple of dipoles $\boldsymbol{d}_A$ and $\boldsymbol{d}_B$ in the Supporting Information of the present contribution. Starting from eq 1, the total intensity can be defined as

$$I^{tot} = \sum_i \rho^i\langle v^i|\boldsymbol{d}^{e}_{Amn}\cdot\boldsymbol{d}^{e}_{Bmn}{}^{*}|v^i\rangle \quad (23)$$

where the summation is performed over all the initial vibrational states i and ρ^i is the Boltzmann population of the initial state $|v^i\rangle$. For OPA and ECD, the initial state is the lowest in energy, while for OPE, it is the highest one.

With these definitions, Supporting Information shows that the spectrum convergence, ς, is given by the relation:

$$\varsigma = \frac{\sum_i\sum_f \rho_{v^i}\langle v^i|\boldsymbol{d}^{e}_{Amn}|v^f\rangle\langle v^f|\boldsymbol{d}^{e}_{Bmn}{}^{*}|v^i\rangle}{\sum_i \rho^i\left[\boldsymbol{d}^{e}_{Amn}(\boldsymbol{Q}^i_0)\cdot\boldsymbol{d}^{e}_{Bmn}{}^{*}(\boldsymbol{Q}^i_0) + \sum_{k=1}^{N}\left(\frac{\partial\boldsymbol{d}^{e}_{Amn}}{\partial Q^i_k}\right)_0\left(\frac{\partial\boldsymbol{d}^{e}_{Bmn}{}^{*}}{\partial Q^i_k}\right)_0\frac{\hbar}{2\omega'_k}(2v'_k + 1)\right]} \quad (24)$$

where $|v^f\rangle$ represents a vibrational final state.

2.3. Implementation. A wide range of approaches to compute vibrationally resolved electronic spectra, for cases where the involved electronic states can be considered not-coupled, has been presented, which differ by their conceptual approach to the transition, vertical, or adiabatic as well as the level of approximation of the respective PESs of the initial and final states, such for example adiabatic FC and adiabatic shift (AS). Additionally, various approximations of the transition dipole moments, FC, FCHT, or HT can be applied. The acronyms AFC, AFCHT, and AHT will be used to refer to the adiabatic model with the harmonic representation of the PES of each electronic state computed at its equilibrium geometry, differing only by the approximation of the transition dipole moment in eq 6, respectively, FC, FCHT, and HT. For the VG and AS models, as stated previously, only the FC approximation will be considered here, as a consequence, the redundant FC suffix will be then omitted. However, it should be noted that present implementation is able to handle transparently FCHT and HT calculations with the VG and AS models. All such models can be combined with computations of one-photon electronic spectra induced by either electric or magnetic transition dipoles or by their mutual interaction. Table 1 provides an overview of the information needed as input for each of the considered models. It is noteworthy that all approaches require the optimized geometry for the initial state along with the calculation of its Hessian matrix. However, they differ significantly for the data required for the final state, whose PES can be built only from the ground of its energy gradient for the simplest VG model or from a full geometry optimization and harmonic analysis for the most demanding one. As a consequence, the choice of the model might have a large impact on the total computational times.

The simplest VG model requires only the energy gradient of the excited state to be calculated at the geometry of the ground state. In a time-dependent perspective, the VG approach is related to the effect of short-term dynamics on the spectra, so it is expected to reproduce well the low-resolution spectrum shape. On the other side, it does not account for the changes in vibrational frequencies and for the normal modes' mixing between the excited and ground electronic states. Because of its characteristics, the VG model provides the most up to date and feasible approach for the studies of the spectrum in a broad energy range and/or for macromolecules. At variance, the AS model requires the determination of the equilibrium structure for the final state but not the frequencies, so it might be considered as a solution for cases where the main interest is in the spectral features close to the transition origin, but no precise frequencies are required. It should be noted that both VG and AS models constrain the total zero-point vibrational energy to be the same in the initial and final states. At variance, they evaluate differently the transition energy between the minima of the initial and final states, which is more accurately computed within the adiabatic framework. However, in both cases, if ZPVE effects are introduced and excited-state frequencies are computed from second deriva-

tives of the excited-state PES, sensible differences can be found, introducing shifts of the final energy levels that are often larger than 0.1 eV.

Finally, the AFC or AFCHT approaches are best suited when an accurate reproduction of the excited-state frequencies, a fine structure of the spectra, and a good estimate for absolute positions of vibronic bands are necessary. However they are rather expensive in terms of computational costs since they involve geometry optimization and Hessian computations in the excited electronic state. Vertical approaches based on a full calculation of the Hessian of the excited state can be convenient in some cases, but they have not been implemented yet and will be the subject of future work. It is worthwhile to note that, in the present implementation, if ab initio computations are performed at the TD-DFT level, then frequency calculations are performed by numerical differentiation of the analytical TD-DFT energy gradients, so the transition dipole electric and magnetic moments as well as their derivatives are directly available from the frequency calculations. However, if analytical second derivatives with respect to the geometrical parameters are available for the method used to compute the energy of the excited electronic state, then the numerical calculation of frequencies must be requested in order to use the Herzberg−Teller approximation of the transition dipole moment. The implementation of the presented computational tool into a general purpose computational package facilitates its use for nonspecialist. However, the presented approach is not limited to quantum mechanical treatments available in the Gaussian package and besides the internal ab initio data user-defined data, e.g. for the vibrational frequencies and/or energies of each electronic state as well as for the transition dipole moments can be provided as input, increasing the flexibility of the implementation. Such a feature is of particular relevance for hybrid approaches where geometries, Hessian computations, and related derivatives of transition dipole moments are obtained at a lower level of theory (e.g., DFT with a medium-size basis set), while energy of electronic transition and related transition dipole moments are further refined by more accurate computations (e.g., DFT with larger basis sets and RI-CC2). Moreover, a number of parameters are then available to fine-tune the spectra layout or to control the prescreening, among others. About the former, it is possible to not only define the spectrum bounds but also the distribution functions used to simulate the spectrum broadening. To this purpose, both Lorentzian, simulating a homogeneous broadening, and Gaussian functions for the inhomogeneous broadening, due to solvent or temperature effects, are available. Moreover, the quality of the spectra simulations is ruled by parameters set for the prescreening method, and various aspects of spectrum convergence with respect to these parameters have been discussed in detail in ref 1. The inclusion of temperature has led to additional functionalities. The two major parameters are the temperature and the minimum Boltzman population (MinPop). The second one sets the minimum population a vibrational state must have with respect to the Boltzmann population of the vibrational ground state (set to 1) to be taken into account as an origin of the transitions. As mentioned before, the initial vibrational states are divided by class and then grouped in sets. Each set is treated independently with a specific total intensity I^{tot} calculated for it. The spectrum convergence as well as the assignment is given for each set. By default, only the final spectrum is printed. However, when needed, specific spectra for each class of the initial and/or final states are available.

In this work, we will mainly concentrate on newly introduced features with respect to the previous Gaussian implementation[1] and discuss the problems related to their applicability to quite different spectroscopic studies, as discussed further in Section 5. The applications presented here are confined to transitions between bound electronic states. Nonetheless, we highlight that the developed methodology and all the different implemented methods can be utilized also for the simulation of photoionization and photoelectron spectra, with the approximation of considering the transition probability independent of the free electron final state and kinetic energy. In this limit, with the current facilities within the Gaussian package, it is possible to obtain the FC envelope of the spectra in arbitrary units.

3. Computational Chemistry Models

The computational chemistry methods have been chosen according to the system under study in order to find a satisfactory balance between feasibility of calculations and accuracy of results. First, a small chiral molecule, *R*-methyloxirane (RMO), has been chosen to assess the computational models, which will be used in further studies, with particular reference to the accuracy of the computed rotatory strengths. For such a reason, the ground and excited electronic state computations have been carried out using DFT and TD-DFT,[23] respectively, with the standard B3LYP,[49] and its longe-range corrected extension CAM-B3LYP,[50,51] functionals in conjunction with N07D,[52,53] N07T,[53,54] and aug-cc-pVTZ basis sets.[55,56] Additionally, for the calculations with CAM-B3LYP, basis sets up to aug-cc-pV5Z have been considered, and their effect on the computed vertical excitation energies and on the rotatory strengths is discussed in the detail. For (*R*)-(+)-3 methylcyclopentanone (R3MCP), we have chosen to apply the CAM-B3LYP/aug-cc-pVDZ computational model, in line with the detailed studies of its ECD spectra by some of us.[5−7,57] Additionally, for R3MCP the convergence of the computed values of the transition dipole moments with respect to the basis set has been evaluated by the comparison of aug-cc-pVDZ results with the N07 double- and triple-ζ, augmented by one set of diffuse functions on the heavy atoms[53] (N07Ddiff and N07Tdiff). For chlorophyll *a*1, the ground-state structure and the harmonic frequencies have been computed with the B3LYP/N07D model, while the forces in first eight singlet excited electronic states have been computed at the TD-DFT level with the CAM-B3LYP[50] functional and the N07D basis set augmented by one set of diffuse functionals on heavy atoms (N07Ddiff), as recommended in excited studies of vinyl radical.[58,59] The vertical excitation energies have been computed as a difference between ground- and excited-state energies computed with CAM-B3LYP/TD-CAM-B3LYP, respectively, with a N07Ddiff basis set, while solvent effects

Table 2. Vertical Electronic Excitations (VE in eV) and Rotatory Strengths (R in cgs Computed with the Length Gauge) Computed For RMO with the TD-CAM-B3LYP Density Functional and Basis Sets Ranging from N07D to aug-cc-pV5Z

		AV5Z	AVQZ	AVTZ	N07Tdiff	N07T	N07Ddiff	N07D
state	exp				VE			
2A	7.07	7.14	7.15	7.15	7.13	7.15	7.15	7.69
3A	7.7	7.46	7.48	7.49	7.46	7.49	7.53	8.04
4A		7.56	7.58	7.58	7.55	7.56	7.61	8.19
5A		7.71	7.73	7.74	7.72	7.72	7.78	8.58
6A	8.5	7.85	7.86	7.86	7.87	7.89	7.89	8.67
7A		8.28	8.30	8.30	8.32	8.32	8.37	8.80
8A		8.32	8.34	8.36	8.36	8.38	8.45	8.95
	exp				R			
2A	−12.56	−15.35	−16.19	−16.63	−16.23	−17.01	−19.89	−3.02
3A[a]	6. 98[a]	−7.40(7.76)	−7.08(9.06)	−6.81(9.73)	−6.46(9.71)	−6.51(9.08)	−3.53(16.13)	3.58(4.85)
4A[a]		8.47	8.64	8.72	8.89	8.75	10.12	10.66
5A[a]		6.69	7.50	7.81	7.27	6.84	9.54	−9.39
6A		10.55	10.87	11.03	10.50	11.04	11.80	14.07
7A		−1.50	−0.11	0.86	0.04	0.72	0.53	−5.86
8A		−15.95	−18.39	−19.83	−16.02	−13.58	−19.74	−18.42

[a] Comparison with experiment is made by summing the transitions to the 3A−5A Rydberg states, shown in parentheses.

on the UV−vis spectrum of chlorophyll *a*1 have been introduced by a polarized continuum medium, as described by the conductor-like polarizable continuum model (CPCM)[60] model. For the OPA and ECD studies of (*Z*)-8-methoxy-4-cyclooctenone (MCO), only the lowest, $\pi^* \leftarrow n$ electronic transition has been considered, thus, the TD-B3LYP/B3LYP//N07Ddiff model, which is able to provide accurate results for the lowest excited states has been applied. All calculations have been performed with a locally modified version of the Gaussian suite of quantum chemistry programs.[61]

4. Validation of the DFT/N07 Model for Computations of ECD Spectra

It is widely recognized[62−65] that computations of ECD spectra are particularly challenging for the quantum mechanical treatments. Hence, the definition of a reliable and feasible computational tool, able to handle studies of ECD spectra, is of relevance to the general applicability of the presented model. Recently, some of us have presented a DFT/N07D model[52,66,67] which has been further validated for a broad range of computational spectroscopy studies: electron spin resonance (ESR), infrared (IR), UV−vis.[58,59] In this work, we have chosen to check the performance of the N07D basis set for the challenging case of ECD spectroscopy as well as the new triple-ζ basis set in the N07 family,[53,54] that is introduced here. In these benchmark studies, we will not only consider the absolute values of the rotatory strengths but also the accuracy of the computed derivatives of the magnetic and electric dipole moments necessary for the inclusion of HT effects into the simulated ECD spectra.

4.1. Computation of Rotatory Strengths for *R*-methyloxirane. RMO stands as a popular example, due to its small size, for the benchmark studies of properties of chiral systems.[63,64,68] In particular, the effect of the basis set on the vertical excitation energies and on the rotatory strengths computed at the B3LYP level with the aug-cc-pVXZ (X = D, T, Q) basis sets (shortly named from now on "AVXZ") has been studied, pointing out the importance of diffuse functions.[63] The results gathered in Table 2 show that all basis sets starting from N07Ddiff predict the vertical excitation energies with a comparable accuracy (within 0.1 eV) and also agree fairy well with the experimental data. Such a finding further confirms the applicability of the N07Ddiff basis to the study of excited states, in line with recent investigations.[58,59] However, as already discussed, computations of rotatory strength are much more demanding with respect to the basis set convergence. It should be noted that none of the theoretical results presented in Table 2, match precisely the experimental values, but such disagreement can be attributed to solvent and vibrational effects as already postulated in previous studies.[63,68] For this reason, we will consider in the following discussion, the results from CAM-B3LYP/aug-cc-pV5Z computations as reference data. It can be observed that the standard N07D basis set is not even sufficient for qualitative studies on the rotatory strength. However, a significant improvement is obtained by adding a set of diffuse functions on heavy atoms, which leads to a semiquantitative agreement, at the expense of slightly more demanding computations. Results can be further improved with the N07T basis set, in particular its augmented version. In fact, the N07Tdiff basis set provides rotatory strengths of accuracy comparable to the much more computationally demanding AVQZ basis set (190 vs 596 basis functions, respectively), and on the whole, closer to the most expensive basis set considered, aug-cc-pV5Z (988 basis functions), than the triple-ζ basis set from the aug-cc-pVXZ family (AVTZ, 322 basis functions). Additionally, we have chosen to test the performance of the standard B3LYP functional for rotational strength computations and to compare the results to the ones obtained with the CAM-B3LYP functional, as the latter provides rotatory strengths in good agreement with experiment, in particular, if sufficiently large basis sets are applied. Results gathered in Table 3 show that, as expected, the B3LYP provides qualitatively correct values only for lower lying excited states of valence character. In conclusion, the results discussed above show that the CAM-B3LYP/N07 model is able to provide qualitatively correct results for all excited electronic states starting with the augmented basis set of double-ζ quality (N07Ddiff), while further refinements

Table 3. Vertical Electronic Excitations (VE in eV) and Rotatory Strengths (R in cgs) Computed for RMO with the TD-CAM-B3LYP and TD-B3LYP Density Functionals and aug-cc-pVTZ and N07Tdiff Basis Sets

		TD-CAMB3LYP		TD-B3LYP	
		N07Tdiff	AVTZ	N07Tdiff	AVTZ
state	exp		VE		
2A	7.07	7.13	7.15	6.53	6.56
3A	7.7	7.46	7.49	6.96	6.99
4A		7.55	7.58	7.00	7.03
5A		7.72	7.74	7.08	7.11
6A	8.5	7.87	7.86	7.37	7.36
7A		8.32	8.30	7.72	7.76
8A		8.36	8.36	7.82	7.82
			R		
2A	−12.56	−16.23	−16.63	−18.76	−19.37
3A[a]	6. 98[a]	−6.46(9.71)	−6.81(9.73)	12.48(15.89)	13.01(16.43)
4A[a]		8.89	8.72	1.20	0.88
5A[a]		7.27	7.81	2.20	2.55
6A		10.5	11.03	8.40	8.80
7A		0.04	0.86	2.67	2.74
8A		−16.02	−19.83	−13.55	−3.50

[a] Comparison with experiment is made by summing the transitions to the 3A−5A Rydberg states, shown in parentheses.

can be introduced by the N07Tdiff one. Additionally, it should be stressed that the B3LYP functional can also be applied to cases where only transitions to the lowest lying electronic states of valence character are considered.

4.2. Accuracy of the Derivatives of the Transition Dipole Moments Computed at The DFT/N07 Levels: Line Shape Convergence of ECD−AFCHT Spectrum for the $S_2 \leftarrow S_0$ Electronic Transition of ax-R3MCP. In the present approach, it is possible to improve the quality of the OPA, OPE, and ECD spectra computed within the AFC approximation by considering changes of the transition dipole moments with the geometry. It has been already mentioned that, as far as the computations of excited electronic state frequencies are performed at the TD-DFT level, the inclusion of the Herzberg−Teller term does not require any additional quantum mechanical calculations with respect to the AFC. For such reason, it should be recommended to perform also FCHT computations whenever possible, in particular, for weakly allowed electronic transitions or for cases when ECD spectra have to be studied. For the latter, it has already been demonstrated that inclusion of the HT term might change the sign of some vibronic lines, as for example, the case of axial-methyl conformer of (*R*)-(+)-3 methylcyclopentanone (ax-R3MCP).[6,57] The higher sensitivity of ECD computations to the transition dipole moment approximation, compared to OPA and OPE, is related to the dot product of two different transition dipole moments and, more precisely, to their relative orientation, which stands as an additional factor. For instance, when the mutual orientation of electric and magnetic dipole moments is close to 90 degrees, small changes might introduce a sign reversal of the computed rotatory strength. For this reason, it is important to check not only how the basis set influences the computed rotatory strength at the equilibrium but also more subtle effects on the accuracy of the computed derivatives of transition dipole moments, which might cause significant changes of the spectral lines. The analysis of the basis set effects on the rotatory strength, presented in Section 4.1, revealed that fairly accurate results are provided by computations with the CAM-B3LYP functional in conjunction with the N07Tdiff basis set. This basis set is small enough to allow the simulation of ECD spectra for medium-size systems with adiabatic approaches, requiring excited electronic state frequency computations. However, having in mind larger systems, it is important to check the performance of the smaller N07Ddiff basis set and to compare these results with CAM-B3LYP/aug-cc-pVDZ computations.[57] When studying the ECD spectrum related to the $S_2 \leftarrow S_0$ electronic transition of the ax-RMCP, it appeared that some of the vibronic transitions changed sign by including the HT term.[6,57] As a consequence, we have chosen ax-RMCP for the benchmark study of the basis set effect on the computed transition dipole moment derivatives and on their influence of the spectra line shape. Panel a in Figure 1 shows the ECD spectra in a $0-4000\ cm^{-1}$ energy range from the transition origin, computed with the three different basis sets under study with the AFC and AFCHT approximations and convoluted with Lorentzian functions with full width at half-maximum (fwhm) of 0.005 eV (in line with previous studies). It is immediately visible that several bands change sign when the HT term is taken into account, and such an effect is consistently obtained for the main spectrum features by all basis sets. Looking more into detail, as shown in panel b of Figure 1 and in the stick spectrum presented in Figure 2, it is possible to find some minor vibronic contributions which differ in sign depending on the basis set. The most visible difference is related to the $\langle 0|2^1\rangle$ transition, where computations at the FCHT level with the aug-cc-pVDZ basis set predicts a negative vibronic band in line with FC approximation, while for the N07 basis sets, its contribution to the spectra is canceled through the HT term. However, despite minor discrepancies, we shall conclude that all studied basis sets provide comparable results for the ECD-FCHT spectra. In particular, the good qualitative agreement obtained with the N07Ddiff basis set justifies its applicability to the studies of vibrationally resolved ECD spectra within the FCHT approximation, which requires expensive computations of the vibrational frequencies in the excited electronic states. It should also be stressed that the hybrid approach with transition dipole moment derivatives computed with basis

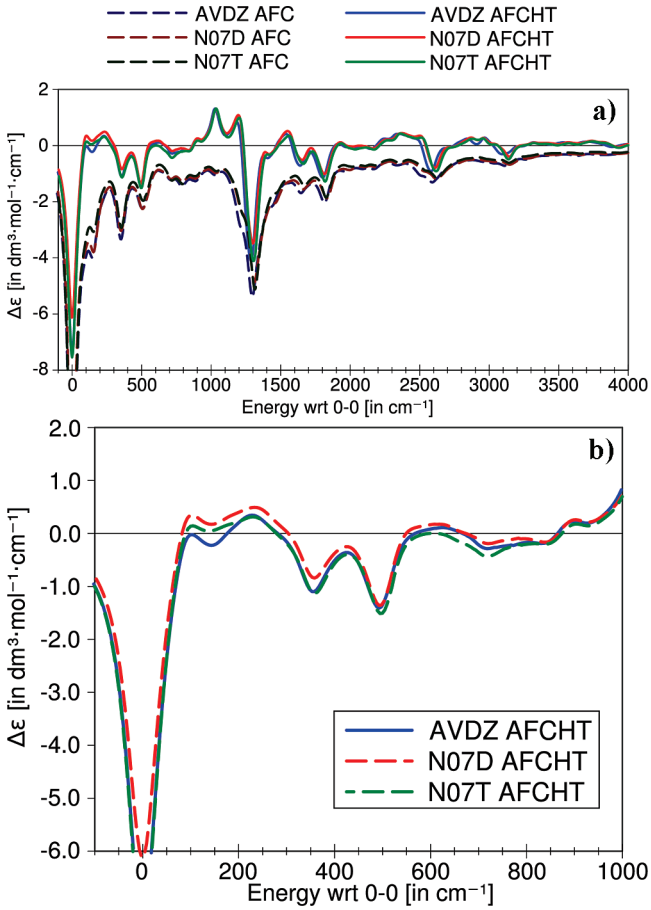

Figure 1. Convergence of the ECD spectrum line shape with respect to the basis set. Accuracy of the derivatives of the transition dipole moments computed at the TD-CAM-B3LYP level with aug-cc-pVDZ (AVDZ), N07Ddiff (N07D), and N07Tdiff (N07T) basis sets. Adiabatic Franck−Condon (AFC) and Franck−Condon Herzberg−Teller approaches (AFCHT) for the $S_2 \leftarrow S_0$ electronic transition of ax-R3MCP (color online). The bands are convoluted with Lorentzian functions of 0.05 eV fwhm and with the spectra span energy range of 0−4000 cm^{-1} (panel a) or 0−1000 cm^{-1} (panel b) with respect to the 0-0 transition.

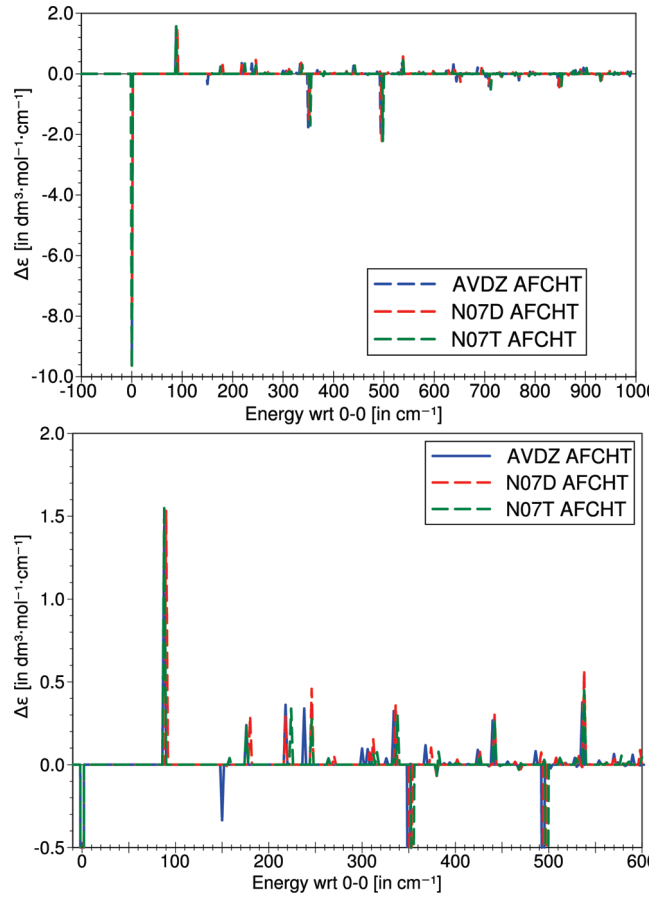

Figure 2. Convergence of the ECD spectrum line shape with respect to the basis set. Accuracy of the derivatives of the transition dipole moments computed at the TD-CAM-B3LYP level with AVDZ, N07D, and N07T basis sets. The stick spectra of the AFCHT for the $S_2 \leftarrow S_0$ electronic transition of ax-R3MCP (color online) span an energy range of 0−1000 cm^{-1} (panel a) or 0−600 cm^{-1} (panel b).

sets of N07D quality, combined with equilibrium properties evaluated at higher level of theory, can offer a noteworthy refinement for larger systems. The current implementation allows such a hybrid scheme through reading of appropriately defined transition dipole moments and their derivatives from the input stream. However, it should be remembered that on the ground of the perturbative HT theory of intensity borrowing,[35] such hybrid approach is not expected to be reliable when the energy gap between the lending and borrowing states change considerably with the basis set.

5. Simulated One-Photon Electronic Spectra

The integrated approach to compute vibrationally resolved one-photon electronic spectra can be applied to a large variety of systems ranging from small molecules in the gas phase to macrosystems in condensed phases, whenever the nonadiabatic couplings are negligible and the harmonic approximation is reliable. In this section, the $S_2 \leftarrow S_0$ one-photon ECD spectra of R3MCP are used to present various aspects of the convergence of the simulated results (Sections 5.1 and 5.2), while the last two subsections: the UV−vis absorption spectrum in the 250−700 nm range of chlorophyll *a*1 (Section 5.3) and the ECD spectrum of the $\pi^* \leftarrow n$ transition of MCO (Section 5.4) are presented in order to illustrate the flexibility of the integrated approach and its applicability to larger systems.

5.1. Vertical and Adiabatic Approaches to Compute Electronic Spectra: Case of OPA, OPE, and ECD Spectra for ax-R3MCP. As already shown in previous sections and discussed in refs 6 and 57, the $S_2 \leftarrow S_0$ electronic transition of the ax-RMCP is an interesting case where HT effects can lead to a change of the sign with respect to the simple FC approach, in case of ECD spectra, but have a lower impact in OPA simulations. Figures 3, 4, and 5 show the simulated OPA, OPE, and ECD spectra obtained with various approximations related to changes between the electronic states within the electronic transition. In fact, for OPA spectra, it is immediately visible that the simplest VG approach yields spectrum line shapes in qualitative agreement with more demanding computations performed within the adiabatic framework, so it can be sufficient to reproduce correctly the general features of the experimental spectra. However, as clearly shown in Figure 4, such an agreement

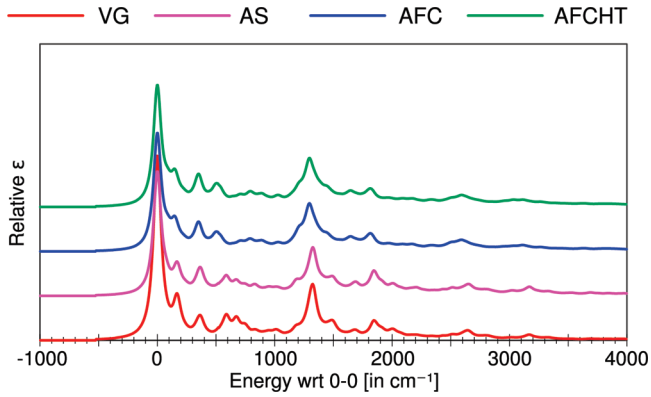

Figure 3. Convoluted OPA spectra of the $S_2 \leftarrow S_0$ electronic transition of ax-R3MCP (color online) computed with vertical and adiabatic approaches: VG, AS, AFC, and AFCHT.

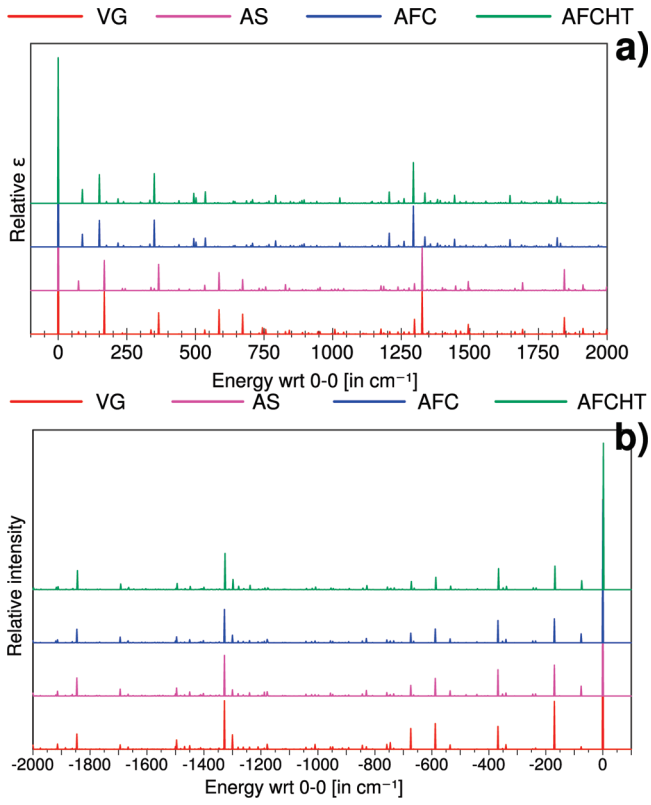

Figure 4. Stick OPA and OPE (panel a and b, respectively) spectra of the $S_2 \leftarrow S_0$ electronic transition of ax-R3MCP (color online) computed with vertical and adiabatic approaches: VG, AS, AFC, and AFCHT.

cannot be expected if the fine structure is also needed. Moreover, larger deviations can be expected for molecules (and/or states) showing larger changes in frequencies and/or significant Duschinsky mixings upon excitation. As an example, in ref 57, sensible differences between VG and AFC results have been documented for the $n \rightarrow \pi^*$ ($S_1 \leftarrow S_0$) electronic transition of both ax- and eq- conformers of RMCP. Such a transition involves the lone pair of the oxygen and the π^* orbital residing on the CO bond, so that the CO stretch is responsible for the most prominent progression of the spectrum, and its vibrational frequency strongly decreases upon excitation. In this situation, models like VG that do not take into account this effect predict too-large spacings

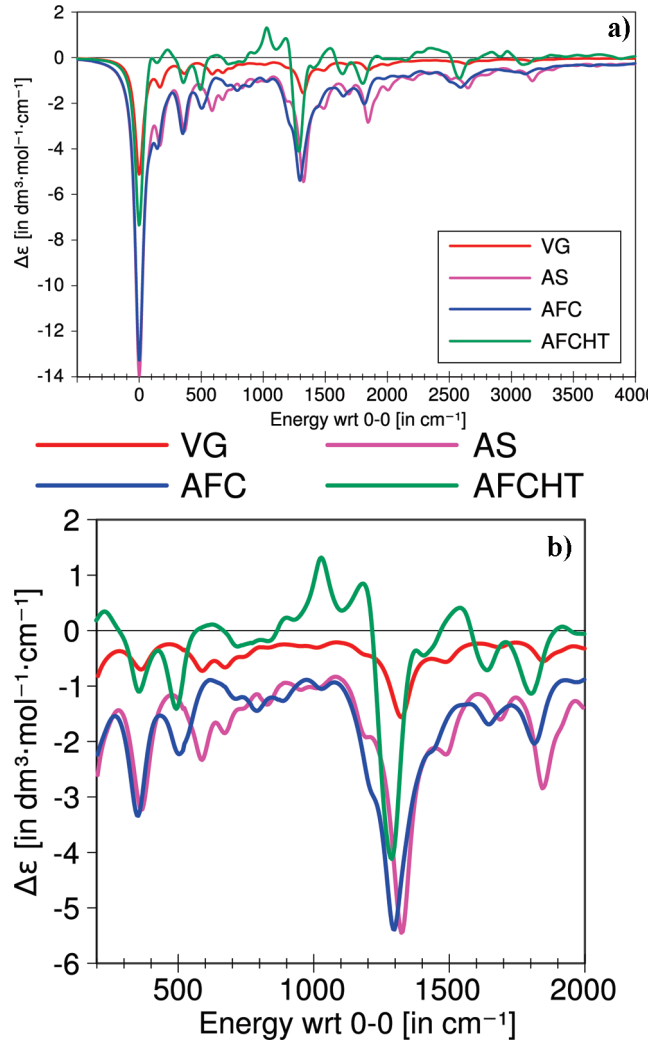

Figure 5. ECD spectra of the $S_2 \leftarrow S_0$ electronic transition of ax-R3MCP computed with vertical and adiabatic approaches: VG, AS, AFC and AFCHT (color online), which span an energy range of 0−4000 cm^{-1} (panel a) or 200−2000 cm^{-1} (panel b) with respect to the 0-0 transition.

between the bands, while application of the AFC model results in a significant improvement of the agreement with the experiments. The situation is different in the case of the OPE spectrum, since the fine structure corresponds to the vibrational frequencies in the ground state, which are correctly taken into account in all models. In fact, panel b of Figure 4 shows that VG, AS, FC, and FCHT predict the same positions for the vibrational transitions. However the general pattern is different, as some bands are missing in VG or varying in intensity.

However, the situation is more complex for ECD spectra; in this case, much more pronounced differences between VG and AS or AFC computations can be observed. In fact, even the AFC and AFCHT spectra line shapes differ significantly when the HT contributions change the sign of some of vibronic transitions, an effect which obviously cannot be reproduced by any FC based approaches: VG, AS, or AFC. Such findings clearly show the higher sensitivity of ECD to the approximation of the transition dipole moment used to compute the spectra. Thus, while VG approaches can be also applied to ECD, the VG-ECD results need to be considered

qualitative at most. It must be noticed that, in ref 5, it has been shown that the VG method with the inclusion of HT effects can reproduce correctly the change in the sign of vibronic transitions, even if differences are visible in the details of the spectrum. Nonetheless, we highlight once more that, at the state-of-the-art level, the computational effort to compute the derivatives of the transition dipole moment is the same as the one required to obtain all the necessary data to compute the spectrum at the AFCHT level, i.e., by fully including all the possible spectral features within the harmonic approximation.

5.2. Temperature Effects and Convergence of Line Shapes for One-Photon Electronic Spectra Simulated in Ambient Conditions. Case of OPA and ECD Spectra for ax-R3MCP. In the current implementation, it becomes possible to include the temperature effects on the spectrum shape, a feature particularly important for the comparison with experimental data performed at ambient conditions. In general, when temperature-dependent spectra are to be simulated by a time-independent approach, like the one pursued here, additional issues arise in choosing the set of vibrational states from which electronic transitions will take place. This choice is defined by the probability of the molecule to be in each initial vibrational state given by its Boltzmann population. Then, a suitable threshold for the minimum population of the vibrational states to be included into the sets considered in computations needs to be chosen. This threshold is defined with respect to the Boltzmann population of the vibrational ground state (set to 1) and can be modified freely (through the MinPop keyword). The intensity and line-shape convergence, with respect to the population threshold, will also be discussed on the examples of OPA−AFC and ECD−AFCHT spectra for the $S_2 \leftarrow S_0$ electronic transition of the ax-RMCP, simulated at 298 K, which are shown in Figures 6 and 7, respectively. It can be immediately observed that temperature has a similar effect in both cases and that the increasing number of initial vibrational states (lower percentage of ground-state Boltzmann population required for state to be included into set) modifies mainly the part of the spectra close to the 0-0 transition, while in the higher energy wing, spectra do not differ significantly from the one computed at 0 K. Additionally, we can note that some temperature effects are already visible even if a limited number of vibrational states is taken into account (MinPop = 25%) and that increasing the number of initial vibrational states leads to a decrease in the intensity of the main transitions, coupled with an increase in intensity for the less pronounced features. Nevertheless, for the AFC approximation, the total spectrum intensity remains constant at the value corresponding to the simulations at 0 K. However, usually the spectrum shape is the property of interest and, as shown in Figure 6, the spectra computed with a minimum population set of 25 and 10% are already quite similar when the intensity with respect to the total Boltzmann population is considered. The latter finding is also valid for ECD spectra, as shown in Figure 7, for which the line-shape convergence does not require the inclusion of a very high number of vibrational initial states, which would, in turn, increase steeply the computational cost. In line with this finding, we have chosen to set to 10% the default value of the Boltzmann population to be considered, however, such a value might be freely modified whenever needed. Nevertheless, it should be noted that in some cases, where normal modes are significantly displaced or noteworthy mixing between them is observed as well as in cases where strong

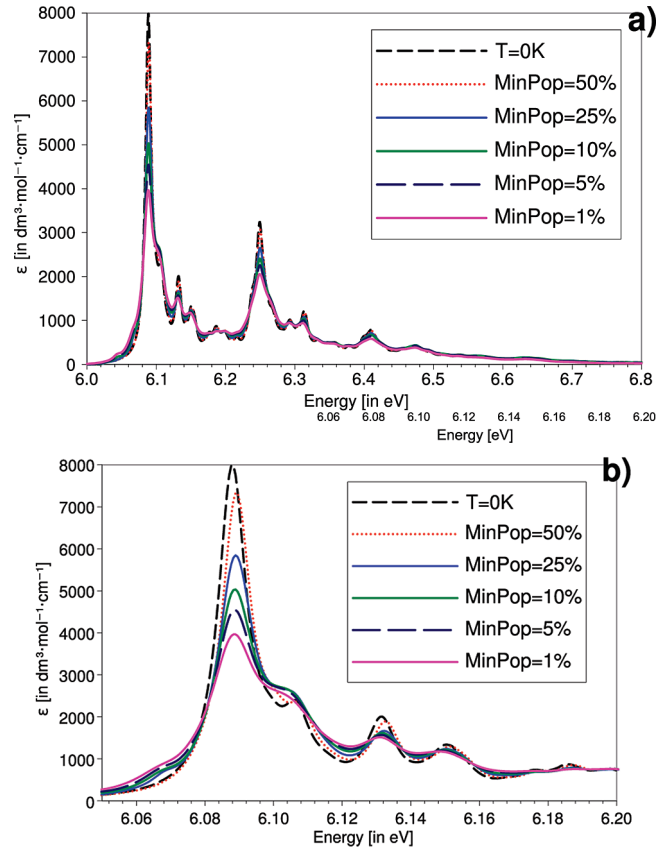

Figure 6. Temperature effects and convergence of the line shapes for one-photon electronic spectra simulated in ambient conditions (298 K) are shown with the case of the OPA spectra of ax-R3MCP (color online), simulated within the AFC framework. The spectra span an energy range of 6.0−6.8 eV (panel a) or 6.06−6.20 eV (panel b).

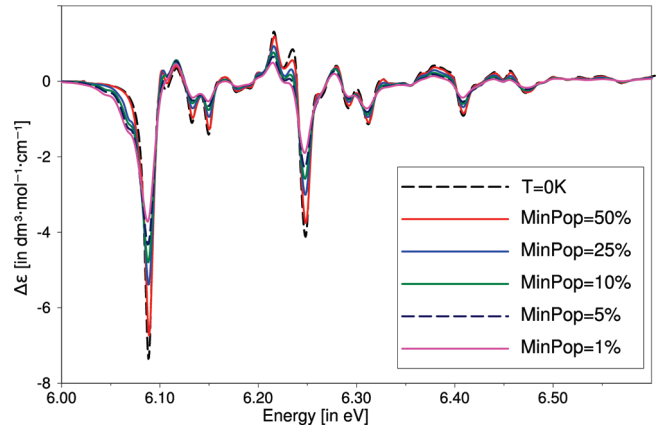

Figure 7. Temperature effects and convergence of the line shapes for one-photon electronic spectra simulated in ambient conditions (298 K) are shown with the case of the ECD spectra of ax-R3MCP (color online), simulated within the AFCHT framework.

progressions are induced by the hot vibrational modes, such a threshold might not be satisfactory.

5.3. UV−vis Spectrum of Chlorophyll *a*1. The understanding of the molecular mechanism of light harvesting in the photosystem II is one of the subjects intensively studied both experimentally and theoretically. For the latter, recent developments within the computational approaches and within the increased computational resources allow, at present, studies at the QM level in ground as well as in excited states. In such a way, a new level of accuracy has become available, and it may be expected that QM computations of optical properties combined with spectroscopic experiments will contribute to shed further light on this phenomenon.[69] In the present work, we have chosen to study the UV−vis spectrum of chlorophyll *a*,[70,71] which has been modeled in the current approach by chlorophyll *a*1, a large molecule with 46 atoms and 132 normal modes. For such a system, fully QM simulations of vibronic spectra within the AFC or AFCHT frameworks are already possible but still computationally demanding, in particular, if large energy windows, encompassing several electronic transitions, need to be studied. This situation can be significantly improved with the VG approach where, to simulate vibrational effects on the spectrum line shape only computations of excited-state forces are required, allowing a relatively cheap and straightforward computation of low-resolution electronic spectra for large molecules in gas phase and in solution. Here, we present such a study for chlorophyll *a*1, for which electronic QM computations have been performed at the DFT/N07D level, and the effect of the methanol solvent has been included by means of the polarizable continuum model, where the solvent is represented by a homogeneous dielectric polarized by the solute and placed within a cavity built as an envelope of spheres centered on the solute atoms.[60] The solvent has been described in the nonequilibrium limit where only its fast (electronic) degrees of freedom are equilibrated with the excited-state charge density, while the slow (nuclear) degrees of freedom remain equilibrated with the ground state. This assumption is well adapted to describe the broad features of the absorption spectrum in solution due to the different time scales of the electronic and nuclear response components of the solvent reaction field.[3]

The simulated UV−vis spectrum in a 250−700 nm range has been obtained by summation of the contributions from transitions to the first eight singlet excited electronic states. It can be noted that the new features of the integrated procedure to compute electronic spectra, which reports results in the absolute values (see Section 2.1) instead of arbitrarily normalized intensity units, allow a more straightforward comparison of relative intensities of vibronic contributions from transitions to different electronic states. Figure 8 shows spectra simulated in a gas phase and a methanol solvent for chlorophyll *a*1, which are compared to the experimental data from the solution.[70,71] It is immediately visible that, while both computed spectra reproduce qualitatively the line shape of their experimental counterpart, a much better agreement, in particular for the absolute positions of vibronic bands, has been obtained for the one simulated in methanol. For the spectrum simulated in methanol solvent, a small 500 cm^{-1}

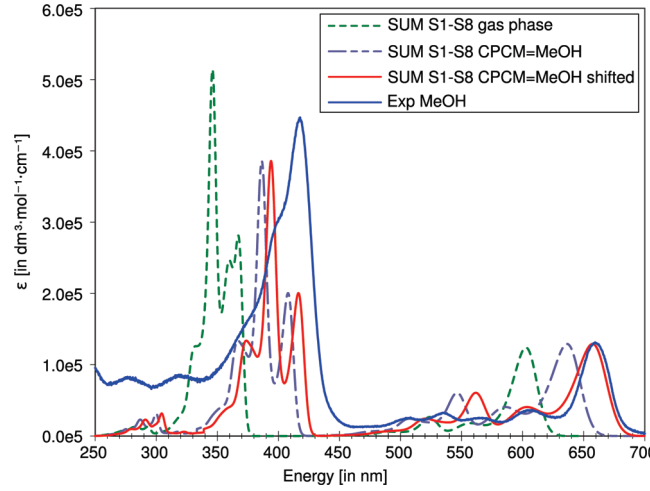

Figure 8. The absorption spectrum of chlorophyll *a*1 in a 250−700 nm energy range, resulting from the sum of the transitions to the eight first singlet electronic states, is simulated in a gas phase and a methanol solution and compared to experimental data obtained in a methanol solvent.[70,71]

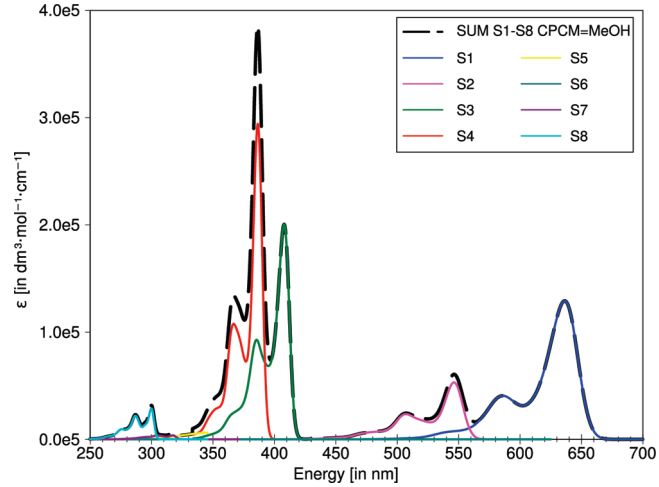

Figure 9. The absorption spectrum of chlorophyll *a*1 (color online) in MeOH (CPCM) in a 250−700 nm energy range is dissected into the contributions of the single transitions.

shift on the energy scale leads to a very good agreement with experiment, and such shifted spectrum is also depicted in Figure 8. For the gas-phase spectrum, the application of a uniform energy shift of 1500 cm^{-1} allows a good match in an energy region around 650 nm, but in this case, the position of most pronounced band is still blue-shifted with respect to the experiment. At this point, we would like to stress that accurate prediction of electronic energies is still a very difficult task even for the most advanced computational approaches, while TD-DFT/DFT//N07D computations have already proven to provide very reasonable estimates of the relative energetics of the electronic states.[58,59] The current study shows also the importance of the direct inclusion of solvent effects, which significantly improve the agreement with experimental data. Additionally, the simulated spectrum can be easily dissected into the single electronic transitions, as shown in Figure 9, allowing to analyze their individual contributions to the spectrum line

shape. In fact, it can be immediately observed that in case of chlorophyll *a*1, the spectrum line shape is dominated by the contributions from transitions to the S1, S3, and S4 excited electronic states, with the non-negligible contributions from transitions to S2 and S8. In line with the general objective of the present work, we will mainly stress the ease and the feasibility of the presented integrated procedure, with results of very good quality obtained by the simple VG approach combined with relatively inexpensive QM studies available through the recently introduced DFT/N07D model. More detailed studies of the spectroscopic properties of chlorophyll *a*1 and of its radical cations are to be reported in a separate work.[72]

5.4. Electronic OPA and ECD Spectrum of (*Z*)-8-Methoxy-4-cyclooctenone. An unusual vibronic pattern in the ECD spectrum has been recently observed for the $\pi^* \leftarrow n$ electronic transition of the enantiopure (*Z*)-8-methoxy-4-cyclooctenone (MCO).[73] In the ECD spectrum, several bands of opposite sign have been observed, at variance with the single broad band found in the absorption spectrum. To analyze this issue, studies in the UV−vis energy range have been performed, aided by IR and VCD experiments and by computations at the DFT level. For the latter, only the vertical transition between the electronic states has been taken into account, and both absorption and ECD spectra have been simulated by applying a phenomenological broadening to the electronic stick data. Several conformers of MCO have been studied theoretically in order to obtain the best match with experimental spectra. On the basis of DFT computations for the ground state performed at the B3LYP/6-311+G(2d,p) level, the simulated IR and VCD spectra have been compared with their experimental counterparts, and the two most stable conformers were identified. However, the contribution from two additional, less stable conformers have been necessary to satisfactorily reproduce the unusual pattern of ECD spectra with the chosen model. It should be noted that our computations performed at the TD-B3LYP/B3LYP//N07diff level agree well with the results presented by Tanaka et al.[73] for the structure and energies of eight MCO conformers. In particular, conformers 1A and 1B are the most stable, and their energies differ only negligibly (within 0.2 kcal/mol), while all other conformers are less stable by at least 2 kcal/mol. Indeed, conformers 1A and 1B show an almost equal stability, so they should be observed in IR and VCD spectra as suggested. Here, we present the OPA and ECD spectra of MCO, which have been simulated considering only one of the two most stable conformers, labeled 1A in ref 71. The simulated absorption and the ECD spectra computed within the AFC and AFCHT frameworks are compared to their experimental counterparts[73] in Figures 10 and 11, respectively. The OPA spectra, depicted in Figure 10, show a single broad band both at the AFC and AFCHT level, in agreement with the experimental findings, and the inclusion of the HT contributions blue-shift the maximum of the computed spectrum improving the agreement with the experiment. Obviously, the same result has been obtained when the AFC approximation has been used for the ECD spectroscopy and, indeed, ECD−AFC is a mirror reflection (due to negative sign of the rotatory strength) of OPA−AFC. At variance, the ECD spectrum computed within the AFCHT framework shows both positive and negative vibronic contributions, in line with experiment. Figure 11 compares the simulated ECD−AFCHT spectrum convoluted with a fwhm of 500 cm^{-1} with the experimental

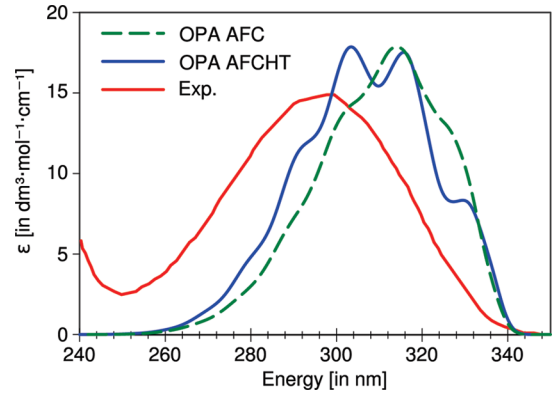

Figure 10. Simulated (at AFC and AFCHT levels) and experimental absorption spectra of the $\pi^* \leftarrow n$ electronic transition of MCO. The theoretical spectra were convoluted with a fwhm of 500 cm^{-1}.

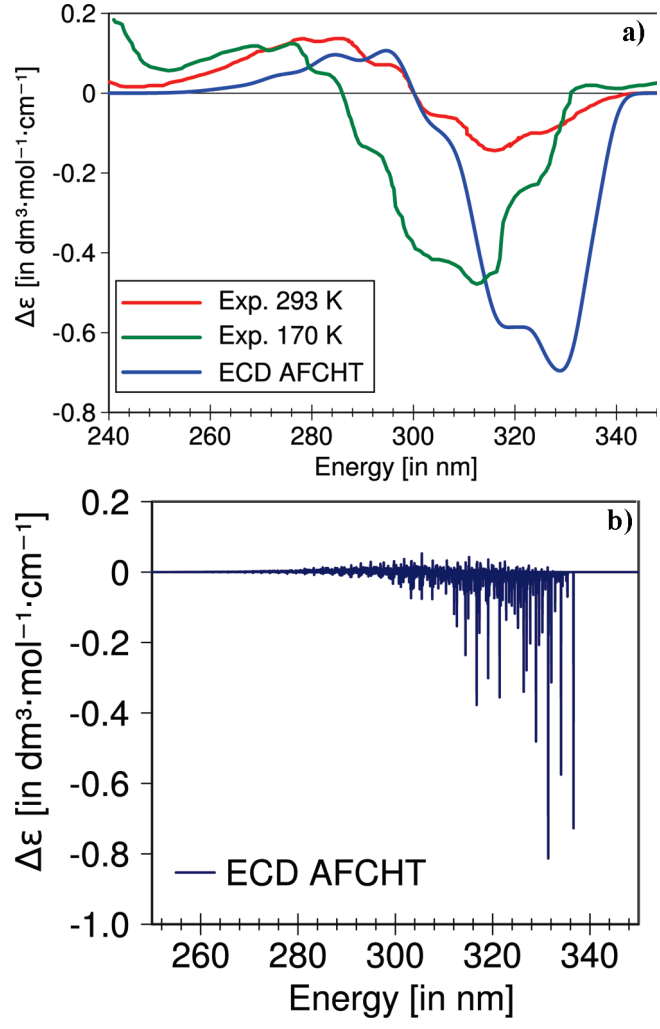

Figure 11. Simulated (at the AFCHT level) and experimental ECD spectra of the $\pi^* \leftarrow n$ electronic transition of MCO. The theoretical spectra were convoluted with a fwhm of 500 cm^{-1}
.

data obtained at room temperature or by cooling the system to 170 K. In panel b of Figure 11, the theoretical stick spectrum is also shown, clearly indicating the presence of positive vibronic contributions. It is noteworthy that the spectrum simulated at 0 K is more similar to its experimental counterpart registered at 170 K than to the one taken at room temperature. More detailed insights of the temperature effects on the OPA and ECD spectra of MCO would require further investigations, which are beyond the scope of the present work. As mentioned above, IR and VCD studies confirmed the presence of another stable structure (1B) at experimental conditions, for which our computations yielded a very small FC integral between the vibrational ground sates. Nevertheless, even if the main spectral features are related to conformer 1A, it should not be excluded that contributions from 1B might slightly modulate the spectrum shape and that taking it into account could further improve the accuracy of the theoretical spectrum, with respect to the experiment. In any case, it should be noted that, within the simplified model where the vibrational effects are neglected,[73] as many as four conformers have been necessary for a qualitative reproduction of the experimental spectra. A change of sign can be sometimes observed in the energy window encompassed by a single electronic state[74] and is often attributed to the contribution of different conformers as in ref 73. However, the issues of possible changes in the sign of some vibronic lines of the ECD spectra due to the HT term have already been demonstrated in refs 6 and 57 and discussed in Section 4.2. Our results suggest that this is also the case for MCO, where the HT contribution indeed influences significantly the spectrum line shape and is necessary for a qualitative agreement with experimental data. Indeed, the simulation of the ECD spectrum within the FCHT framework can describe all its unusual features considering only the most stable isomer, at variance with the previous studies based on simple ECD spectra, simulated by applying a phenomenological broadening to the electronic stick data.

Conclusions

A general approach for the simulation of vibrationally resolved one-photon electronic spectra has been implemented and applied to a variety of molecular systems, showing the high flexibility of the developed computational tool. The integration of all procedures within the same computational package allows for the fully automatic computation of vibrationally resolved electronic spectra. Despite the fact that our computational scheme has been tailored for large systems, it can be utilized as well to generate high-quality spectra for small systems, when nonadiabatic and anharmonic couplings are negligible, since it allows different levels of approximation for the computation of FC integrals. It should be noted that, even when nonadiabatic couplings can be neglected, several issues which are of general importance in many cases remain still open, like problems related to the presence of double-well potentials, large molecular displacements, or multimode couplings. However, all these issues are, in more general terms, related to the anharmonicity, and as we already stated, the simulations of vibrationally resolved electronic spectra with anharmonic models appropriately tailored for vibronic transitions are under active development. Notwithstanding the above limitations, we point out that, in the present work, we introduce an easy-to-use, general, and robust computational tool able to simulate good-quality spectra even for large systems with hundreds of normal modes, whenever harmonic approximation is reliable, paving the route to spectroscopic studies of systems of direct biological and/or technological interest, improving their interpretation and understanding.

Acknowledgment. This work was supported by Italian MIUR (PRIN 2006) and CNR (PROMO 2006). The large scale computer facilities of the VILLAGE network (http://village.unina.it) are kindly acknowledged.

Supporting Information Available: The generalized calculation of the spectrum convergence (I^{calc}/I^{tot}) for any couple of dipoles $\boldsymbol{d}_A$ and $\boldsymbol{d}_B$. This material is available free of charge via the Internet at http://pubs.acs.org.

References

(1) Barone, V.; Bloino, J.; Biczysko, M.; Santoro, F. *J. Chem. Theory Comput.* **2009**, *5*, 540–554.

(2) Frisch, M. J.; Trucks, G. W.; Schlegel, H. B.; Scuseria, G. E.; Robb, M. A.; Cheeseman, J. R.; Scalmani, G.; Barone, V.; Mennucci, B.; Petersson, G.; Nakatsuji, H.; Caricato, M.; Li, X.; Hratchian, H. P.; Izmaylov, A. F.; Bloino, J.; Zheng, G.; Sonnenberg, J. L.; Hada, M.; Ehara, M.; Toyota, K.; Fukuda, R.; Hasegawa, J.; Ishida, M.; Nakajima, T.; Honda, Y.; Kitao, O.; Nakai, H.; Vreven, T.; Montgomery, J. A.; Peralta, J. E.; Ogliaro, F.; Bearpark, M.; Heyd, J. J.; Brothers, E.; Kudin, K. N.; Staroverov, V. N.; Kobayashi, R.; Normand, J.; Raghavachari, K.; Rendell, A.; Burant, J.; Iyengar, S. S.; Tomasi, J.; Cossi, M.; Rega, N.; Millam, J. M.; Klene, M.; Knox, J. E.; Cross, J. B.; Bakken, V.; Adamo, C.; Jaramillo, J.; Gomperts, R.; Stratmann, R. E.; Yazyev, O.; Austin, A. J.; Cammi, R.; Pomelli, C.; Ochterski, J. W.; Martin, R. L.; Morokuma, K.; Zakrzewski, V. G.; Voth, G. A.; Salvador, P.; Dannenberg, J. J.; Dapprich, S.; Parandekar, P. V.; Mayhall, N. J.; Daniels, A. D.; Farkas, O.; Foresman, J. B.; Ortiz, J. V.; Cioslowski, J.; Fo, D. J. *Gaussian 09, Revision A.2*, Gaussian Inc.: Wallingford, CT, 2009.

(3) Santoro, F.; Improta, R.; Lami, A.; Bloino, J.; Barone, V. *J. Chem. Phys.* **2007**, *126*, 084509/1−13.

(4) Santoro, F.; Lami, A.; Improta, R.; Bloino, J.; Barone, V. *J. Chem. Phys.* **2008**, *128*, 224311/1−17.

(5) Lin, N.; Luo, Y.; Santoro, F.; Zhao, X.; Rizzo, A. *Chem. Phys. Lett.* **2008**, *464*, 144–149.

(6) Santoro, F.; Barone, V. *Int. J. Quantum Chem.* **2010**, *110*, 476–486.

(7) Lin, N.; Santoro, F.; Rizzo, A.; Luo, Y.; Zhao, X.; Barone, V. *J. Phys. Chem. A* **2009**, *113*, 4198–4207.

(8) Bloino, J.; Biczysko, M.; Crescenzi, O.; Barone, V. *J. Chem. Phys.* **2008**, *128*, 244105/1−15.

(9) de Groot, M.; Buma, W. J. *Chem. Phys. Lett.* **2007**, *435*, 224–229.

(10) de Groot, M.; Buma, W. J. *Chem. Phys. Lett.* **2006**, *420*, 459–464.

(11) Dierksen, M.; Grimme, S. *J. Chem. Phys.* **2004**, *120*, 3544/1−11.

(12) Pugliesi, I.; Tonge, N. M.; Hornsby, K. E.; Cockett, M. C. R.; Watkins, M. J. *Phys. Chem. Chem. Phys.* **2007**, *9*, 5436–5445.

(13) Tonge, N. M.; MacMahon, E. C.; Pugliesi, I.; Cockett, M. C. R. *J. Chem. Phys.* **2007**, *126*, 154319/1−11.

(14) Hazra, A.; Chang, H. H.; Nooijen, M. *J. Chem. Phys.* **2004**, *121*, 2125/1−12.

(15) Köppel, H.; Domcke, W.; Cederbaum, L. S. *Adv. Chem. Phys.* **1984**, *57*, 59–246.

(16) Köppel, H.; Domcke, W.; Cederbaum, L. The Multi-mode vibronic-coupling approach In *Conical Intersections, Electronic Structure, Dynamics and Spectroscopy*; World Scientific Publishing Co.: Singapore, 2004; pp 323−368.

(17) Nooijen, M. *Int. J. Quantum Chem.* **2006**, *106*, 2489–2510.

(18) Beck, H.; Jäckle, A.; Worth, G.; Meyer, H.-D. *Phys. Rep.* **2000**, *324*, 1–105.

(19) Christopher, P. S.; Shapiro, M.; Brumer, P. *J. Chem. Phys.* **2006**, *124*, 184107/1−11.

(20) Macak, P.; Luo, Y.; Ågren, H. *Chem. Phys. Lett.* **2000**, *330*, 447–456.

(21) Borrelli, R.; Peluso, A. *J. Chem. Phys.* **2006**, *125*, 194308/1−8.

(22) Peluso, A.; Borrelli, R.; Capobianco, A. *J. Phys. Chem. A* **2009**, *113*, 14831–14837.

(23) Scalmani, G.; Frisch, M. J.; Menucci, B.; Tomasi, J.; Cammi, R.; Barone, V. *J. Chem. Phys.* **2006**, *124*, 094107/1−15.

(24) Furche, F.; Ahlrichs, R. *J. Chem. Phys.* **2004**, *121*, 12772/1−2.

(25) Köhn, A.; Hättig, C. *J. Chem. Phys.* **2003**, *119*, 5021/1−16.

(26) Kemper, M.; Van Dijk, J.; Buck, H. *Chem. Phys. Lett.* **1978**, *53*, 121–124.

(27) Berger, R.; Fischer, C.; Klessinger, M. *J. Phys. Chem. A* **1998**, *102*, 7157–7167.

(28) Dierksen, M.; Grimme, S. *J. Chem. Phys.* **2005**, *122*, 244101/1−9.

(29) Santoro, F.; Lami, A.; Improta, R.; Barone, V. *J. Chem. Phys.* **2007**, *126*, 184102/1−11.

(30) Jankowiak, H.-C.; Stuber, J. L.; Berger, R. *J. Chem. Phys.* **2007**, *127*, 234101/1−23.

(31) IDEA: In-Silico Developments for Emerging Applications; http://idea.sns.it. Accessed January 29, 2010.

(32) Eckart, C. *Phys. Rev.* **1937**, *47*, 552–558.

(33) Franck, J. *Trans. Faraday Soc.* **1926**, *21*, 536–542.

(34) Condon, E. U. *Phys. Rev.* **1928**, *32*, 858–872.

(35) Herzberg, G.; Teller, E. *Z. Phys. Chem. B-Chem. E* **1933**, *21*, 410–446.

(36) Luis, J. M.; Bishop, D. M.; Kirtman, B. *J. Chem. Phys.* **2004**, *120*, 813–822.

(37) Luis, J. M.; Torrent-Sucarrat, M.; Sola, M.; Bishop, D. M.; Kirtman, B. *J. Chem. Phys.* **2005**, *122*, 184104/1−13.

(38) Duschinsky, F. *Acta Physicochim. URSS* **1937**, *7*, 551–566.

(39) Sharp, T. E.; Rosenstock, H. M. *J. Chem. Phys.* **1963**, *41*, 3453–3463.

(40) Islampour, R.; Dehestani, M.; Lin, S. H. *J. Mol. Spectrosc.* **1999**, *194*, 179–184.

(41) Mebel, A. M.; Hayashi, M.; Liang, K. K.; Lin, S. H. *J. Phys. Chem. A* **1999**, *103*, 10674–10690.

(42) Kikuchi, H.; Kubo, M.; Watanabe, N.; Suzuki, H. *J. Chem. Phys.* **2003**, *119*, 729–735.

(43) Liang, J.; Li, H. *Mol. Phys.* **2005**, *103*, 3337–3342.

(44) Chang, J.-L. *J. Chem. Phys.* **2008**, *128*, 174111/1−10.

(45) Cederbaum, L. S.; Domcke, W. *J. Chem. Phys.* **1976**, *64*, 603–611.

(46) Doktorov, E. V.; Malkin, I. A.; Man'ko, V. I. *J. Mol. Spectrosc.* **1977**, *64*, 302–326.

(47) Ruhoff, P. T. *Chem. Phys.* **1994**, *186*, 355–374.

(48) Malmqvist, P.-Å.; Forsberg, N. *Chem. Phys.* **1998**, *228*, 227–240.

(49) Becke, D. *J. Chem. Phys.* **1993**, *98*, 5648–5652.

(50) Yanai, T.; Tew, D. P.; Handy, N. C. *Chem. Phys. Lett.* **2004**, *393*, 51–57.

(51) Peach, M. J. G.; Helgaker, T.; Salek, P.; Keal, T. W.; Lutnaes, O. B.; Tozer, D. J.; Handy, N. C. *Phys. Chem. Chem. Phys.* **2006**, *8*, 558–562.

(52) Barone, V.; Cimino, P.; Stendardo, E. *J. Chem. Theory Comput.* **2008**, *4*, 751–764.

(53) Double and triple- ζ basis sets of N07 family, N07D, N07T and N07Tdiff; IDEA: In-Silico Developments for Emerging Applications; http://idea.sns.it. Accessed January 29, 2010.

(54) Barone, V. to be published.

(55) Dunning, T. H. *J. Chem. Phys.* **1989**, *90*, 1007–1023.

(56) Kendall, R.; Dunning, T., Jr.; Harrison, R. *J. Chem. Phys.* **1992**, *96*, 6769–6806.

(57) Lin, N.; Santoro, F.; Zhao, X.; Rizzo, A.; Barone, V. *J. Phys. Chem. A* **2008**, *112*, 12401–12411.

(58) Barone, V.; Bloino, J.; Biczysko, M. *Phys. Chem. Chem. Phys.* **2010**, *12*, 1092–1101.

(59) Barone, V.; Biczysko, M.; Cimino, P. Interplay of stereo electronic vibrational and environmental effects in tuning physico-chemical properties of carbon centered radicals. In *Carbon-Centered Free Radicals and Radical Cations*; Forbes, M. D. E., Ed.; John Willey & Sons, Inc.: Hoboken, NJ, 2010; pp 105−139.

(60) Cossi, M.; Scalmani, G.; Rega, N.; Barone, V. *J. Comput. Chem.* **2003**, *24*, 669–681.

(61) Frisch, M. J.; Trucks, G. W.; Schlegel, H. B.; Scuseria, G. E.; Robb, M. A.; Cheeseman, J. R.; Scalmani, G.; Barone, V.; Mennucci, B.; Petersson, G.; Nakatsuji, H.; Caricato, M.; Li, X.; Hratchian, H. P.; Izmaylov, A. F.; Bloino, J.; Zheng, G.; Sonnenberg, J. L.; Hada, M.; Ehara, M.; Toyota, K.; Fukuda, R.; Hasegawa, J.; Ishida, M.; Nakajima, T.; Honda, Y.; Kitao, O.; Nakai, H.; Vreven, T.; Montgomery, J. A.; Peralta, J. E.; Ogliaro, F.; Bearpark, M.; Heyd, J. J.; Brothers, E.; Kudin, K. N.; Staroverov, V. N.; Kobayashi, R.; Normand, J.; Raghavachari, K.; Rendell, A.; Burant, J.; Iyengar, S. S.; Tomasi, J.;; Cossi, M.; Rega, N.; Millam, J. M.; Klene, M.; Knox, J. E.; Cross, J. B.; Bakken, V.; Adamo, C.; Jaramillo, J.; Gomperts, R.; Stratmann, R. E.; Yazyev, O.; Austin, A. J.; Cammi, R.; Pomelli, C.; Ochterski, J. W.; Martin, R. L.; Morokuma, K.; Zakrzewski, V. G.; Voth, G. A.; Salvador, P.; Dannenberg, J. J.; Dapprich, S.; Parandekar, P. V.; Mayhall, N. J.; Daniels, A. D.; Farkas, O.; Foresman, J. B.; Ortiz, J. V.; Cioslowski, J.; Fo, D. J. *Gaussian Development*

Version, Revision H.05, Gaussian, Inc.: Wallingford, CT, 2006.

(62) Grimme, S.; Diedrich, C. *J. Phys. Chem. A* **2003**, *107*, 2524–2539.

(63) Pecul, M.; Ruud, K.; Helgaker, T. *Chem. Phys. Lett.* **2004**, *388*, 110–119.

(64) Crawford, D. T.; Tam, M. C.; Abrams, M. L. *J. Phys. Chem. A* **2007**, *111*, 12057–12068.

(65) Grimme, S.; Goerigk, L. *J. Phys. Chem. A* **2009**, *113*, 767–776.

(66) Barone, V.; Cimino, P. *Chem. Phys. Lett.* **2008**, *454*, 139–143.

(67) Barone, V.; Cimino, P. *J. Chem. Theory Comput.* **2009**, *5*, 192–199.

(68) Pecul, M.; Marchesan, D.; Ruud, K.; Coriani, S. *J. Chem. Phys.* **2005**, *122*, 024106/1−9.

(69) Vassiliev, S.; Bruce, D. *Photosynth. Res.* **2008**, *97*, 75–89.

(70) Du, H.; Fuh, R. A.; Li, J.; Corkan, A.; Lindsey, J. S. *Photochem. Photobiol.* **1998**, *68*, 141–142.

(71) Strain, H. H.; Thomas, M. R.; Katz, J. J. *Biochim. Biophys. Acta* **1963**, *75*, 306–311.

(72) Biczysko, M.; Borkowska, M.; Bloino, J.; Barone, V. in preparation.

(73) Tanaka, T.; Oelgemoller, M.; Fukui, F.; Aoki, F.; Mori, T.; Ohno, T.; Inoue, Y. *Chirality* **2007**, *19*, 415–427.

(74) Pescitelli, G.; Di Bari, L.; Caporusso, A. M.; Salvadori, P. *Chirality* **2008**, *20*, 393–399.

CT9006772